CHAPTER 1

INTRODUCTION

1.1 Background

In the problem of high-cycle fatigue, fatigue life is generally determined by the number of cycles until the occurrence of a fatigue crack of several mm in length. Thus, a small crack is used to indicate the fatigue limit state of steel members. This concept would be appropriate to the fatigue design for newly constructed steel structures. However, it is difficult to apply the concept of fatigue limit state to all fatigue damages in existing steel bridges, because the numbers of fatigue damages have already amounted to a huge number, while available budget and manpower decease gradually. On the other hand, among the fatigue cracks, some cracks appear at secondary steel members, or the crack propagation is under the retention state. The risk of fatigue damage is different according to the stress condition of steel member. Therefore, for reasonable maintenance, it is essential to determine a countermeasure for each fatigue damage based on an understanding of the damage mechanism.

Crack propagation analysis based on fracture mechanics has mainly focused on small cracks, and a number of studies have proven its accuracy. A short crack which penetrates the plate thickness is taken as the fatigue limit state, however, some cracks can continue propagating, and reach to complicated stress field. It is questionable to apply this concept to maintenance of existing steel bridges. Further studies should be performed to simulate the propagation behavior of relatively long fatigue cracks.

Some long fatigue cracks have been reported in steel bridges. In Japan, as shown in **Fig.1.1**, long through-thickness fatigue cracks have been detected and have gradually increased in orthotropic steel decks (JRA, 2002; Yuge et al., 2004; Miki, 2005; Xiao et al., 2008; Ya, 2008). Among them, two types generally originate from repeated

out-of-plane bending due to repeated wheel loads: fatigue cracks at the welded joint between deck plate and vertical stiffener, and at the welded joint between deck plate and trough rib. Out-of-plane bending results in high local flexural stresses in the deck plate and trough rib, because the thicknesses of the deck plate and the trough rib are relatively thin.

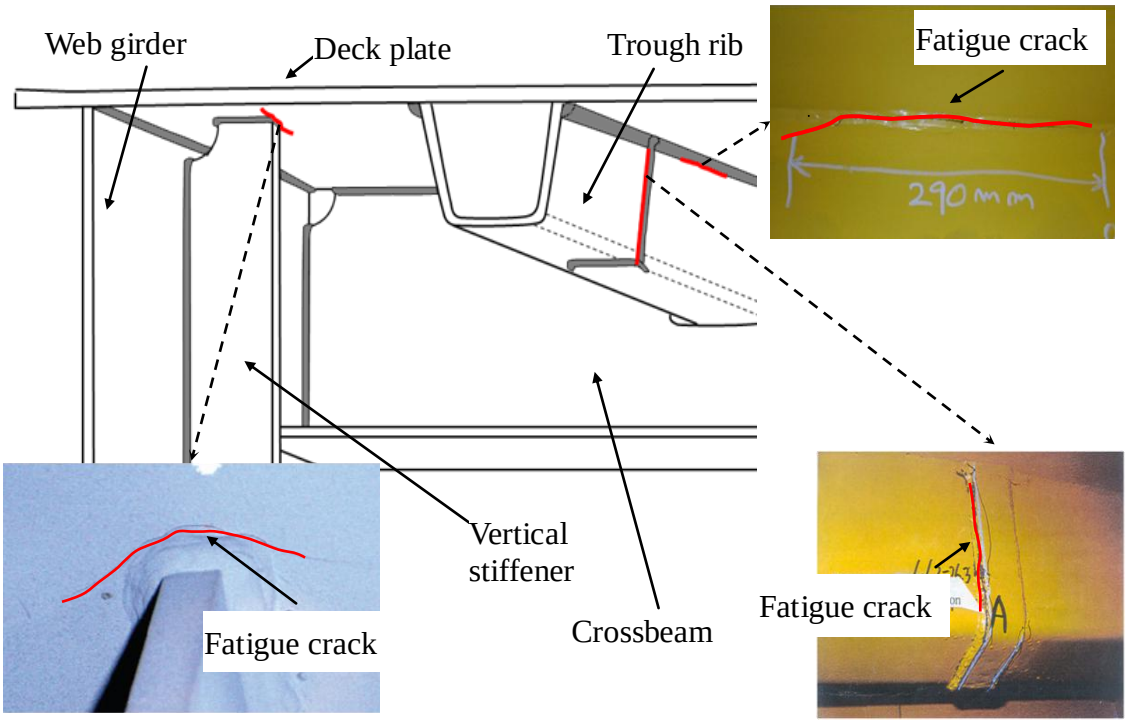

Fig 1.1 Through-thickness fatigue cracks in orthotropic steel deck

Many efforts have been made by some researchers to clarify the propagation behavior of through-thickness fatigue cracks subjected to tension by experimental and numerical analysis studies. The estimation equation of stress intensity factor (SIF), which is an important factor to determine the crack growth, had been established as well. The stress distribution under tension is uniform in the plate thickness direction, but the out-of-plane bending condition causes some difficulties in predicting the crack propagation due to the gradient stress and the crack closure on the compressive side. Some researchers have performed experiments and numerical analysis studies on through-thickness cracking under out-of-plane bending, and they have also proposed a simple estimating equation for SIF. In the previous studies, the SIF under out-of-plane

bending was obtained under the assumption that the crack front was straight in the plate thickness direction. However, under out-of-plane bending conditions, the crack growth rate along the crack front would vary due to the gradient stress and the crack closure on the compressive side. In addition, the analyses of previous studies were carried out on relatively short through-thickness cracks. For these reasons, it is questionable to apply the results to long through-thickness cracks. This study made efforts to establish the simulation technique for long through-thickness fatigue cracking under out-of-plane bending.

1.2 Previous research

1.2.1 Crack propagation behavior

1) Stress intensity factor

Linear elastic fracture mechanics (LEFM) is a classical approach to estimate fatigue crack propagation, life, and growth behavior. This approach quantitatively defines the severity of damage near the crack tip according to estimation of crack propagation by stress intensity factor (SIF) proposed by Irwin (1957). The SIF is determined depending on geometry configuration, loading condition, and crack shape. Newman and Raju (1981) developed an equation to estimate the SIF of a semi-elliptical surface crack in tension and bending.

Paris and Erdogan (1963) have established the correlation between the fatigue crack growth rate and the SIF range as follows,

$$\frac{da}{dN} = C(\Delta K)^m \qquad (1.1)$$

where, C and m are material constants; ΔK is SIF range which is affected by crack geometries and applied load, etc. a and N are crack length and number of fatigue cycles, respectively.

The SIF is the essential parameter to identify the crack growth behavior. Many researchers have undertaken efforts to evaluate the SIF. A common numerical method is the displacements extrapolation method (Owen, 1983), wherein the SIF can be calculated by extrapolating the displacements adjacent to the crack tip. Another common method is J-integral method (Rice, 1968), wherein the SIF is directly related to the energy release rate, which is equal to the path independent J-integral. Additionally, there are other methods to estimate the SIF. The stress method (Broek, 1986; Murakami, 1987) uses the stress directly to calculate the SIF. The nodal force method (Raju, 1979) calculates the SIF based on the nodal forces. The virtual crack closure-integral method (Rybicki, 1977) computes the SIF based on the nodal forces and displacements.

2) Direction of crack propagation

In order to predict the direction of crack propagation, several fracture criteria have been proposed. Typical crack criteria include the maximum circumferential stress (MCS) criterion (Erdogan and Sih, 1963); the minimum strain energy density (MSED) criterion (Sih et al., 1974); and the maximum energy release rate (MERR) criterion (Hussain et al., 1974; Palaniswamy et al., 1978). The MCS criterion assumes that the fracture occurs in the direction where the circumferential stress is the maximum around the crack tip. The MSED criterion states that the fracture occurs in the direction where the strain energy density becomes the minimum. The MERR criterion assumes that a fracture is generated in the direction where the energy release rate is the maximum.

In fracture mechanics, three modes of cracking are defined based on the deformation of the crack illustrated in **Fig. 1.2.** Mode I is opening mode; Mode-II is sliding mode; and Mode-III is tearing mode. The MCS criterion is only applicable to the mixed-mode I/II conditions. In the MSED criterion, the SIF of mode-III has an effect on the equivalent SIF of the three modes, but has no effect on predicted crack direction, so it is not applicable to three-mode mixed conditions. On the other hand, the MERR criterion has a reasonable basis of energy balance and is suitable to apply to a three-mode mixed crack.

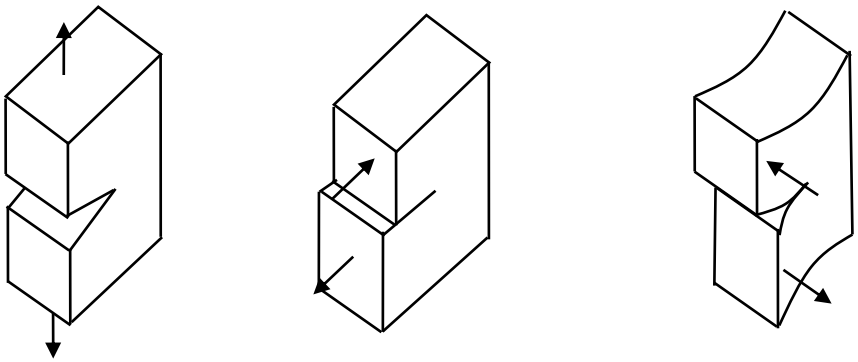

<Mode-I (Opening mode)> <Mode-II (Sliding mode)> <Mode-III (Tearing mode)>

Fig. 1.2 Three modes of cracking

1.2.2 Through-thickness cracks

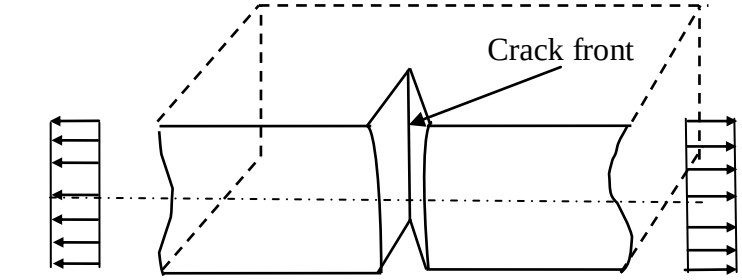

a) In-plane tension

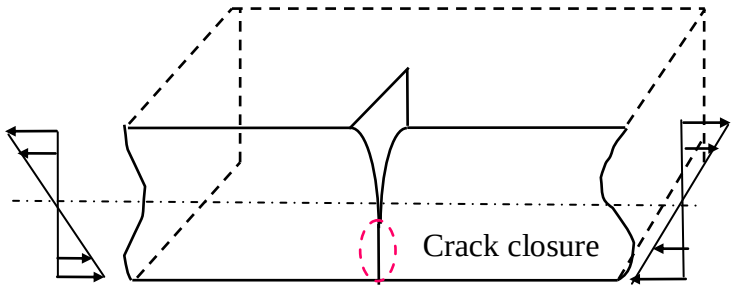

b) Out-of-plane bending

Fig.1.3 Through-thickness cracked plate

Most research on through-thickness cracks has addressed the axial tensile loading condition, in which the stress distribution through the plate thickness direction is uniform. (Newman et al., 1984; Bakker et al., 1992; Kwon et al., 2000; Su et al., 1996; Hwang et al., 2004; Wu, 2006; Branco et al., 2008). In this research, the shape of crack

front was assumed to be a straight line, which was perpendicular to the plate surface as illustrated in **Fig. 1.3 a)**. Hereafter, the shape will be called '*straight line*'.

In order to estimate the SIF of the through-thickness crack under tension, Tada and Irwin (1973) proposed a simple equation as follows: Equation (1.2)

$$K = \sigma\sqrt{\pi a}\sqrt{\frac{2B}{\pi a}tan\frac{\pi a}{2B}} \qquad (1.2)$$

where, σ is nominal stress, *a* is crack length, and *B* is half of plate width.

On the other hand, out-of-plane bending brings some difficulties in predicting crack behavior because of the non-uniform stress distribution along the plate thickness shown in **Fig.1.3 b)**. SIF distribution along the crack front is not uniform due to the stress gradient and the crack closure on the compression side.

Williams (1961) performed the numerical analysis research on the SIF of through-thickness cracking under out-of-plane bending by plate theory. Many researchers (Sih et al., 1966; Hartranft et al., 1969; Folias et al., 1975) have since obtained improved methods to calculate the SIF, but all the analytical models assumed the crack faces to be free surfaces and ignored the crack closure on the compressive side. John et al. (1975) presented numerical solutions for stresses and displacements near the crack front by considering the crack closure based on Kirchhoff's boundary condition. However, crack closure was only applied along the compressive plate surface, while the actual crack closure had a certain height in the thickness direction as shown in **Fig.1.3 b)**. Alwar et al. (1983) and Kwon et al. (1989) introduced an analytical model in which the crack surfaces make contact over an area on the compression side and identified the influence of crack closure on the variation of SIF through the plate thickness.

In order to establish a simple equation to calculate the SIF of through-thickness cracks under out-of-plane bending, Erdogan and Roberts (1965) carried out a comparative investigation on the crack propagation behavior in in-plane tension and out-of-plane bending. The equation for calculating the SIF in out-of-plane bending was

theoretically deduced based on Eq. (1.1).

The effect of out-of-plane bending was calculated by introducing a correction factor α, as in Equation (1.3)

$$K_{bending} = \alpha\sigma\sqrt{\pi a}\sqrt{\frac{2B}{\pi a}tan\frac{\pi a}{2B}} \qquad (1.3)$$

The correction factor α was set at 0.5, meaning that the crack growth rate under tension is two times larger than that under out-of-plane bending.

They also verified the theoretical deduction by comparing the test results performed on a thin steel plate (less than 5 mm thickness). The experimental results agreed well with the theoretical results. However, the theoretical model assumed that the crack-front shape was a straight line. Kanazawa and Machida (1974) theoretically analyzed the characteristics for crack propagation of a through-thickness crack under the combined load of in-plane tension and out-of-plane bending by assuming the equivalence of the plastic zone size. They defined the effective SIF as the criterion of fatigue crack propagation for the through-thickness crack under the combined load of in-plane tension and out-of-plane bending. The effectiveness of the criterion was confirmed by a fatigue crack propagation test. However, the crack-front shape was also assumed to be straight, and the crack closure in the compressive side was neglected.

1.2.3 Through-thickness cracks at rib-to-deck welded joints

Generally, as shown in **Fig.1.4,** two kinds of fatigue cracks have been observed at the welded joint between trough rib and deck plate (called '*rib-to-deck welded joint*' hereafter). One is the *root-deck crack* initiated from the weld root and propagated into the deck plate, and the other is the *root-weld crack* initiated from the weld root and propagated into the weld bead through the weld throat. Compared with the *root-weld* crack, the *root-deck* crack was detected more frequently in experiments. Therefore, most of the research (Tsakopoulos et al., 2003; Miki, 2005; Xiao et al., 2008; Sim et al., 2009; Izumi et al., 2010) on fatigue cracks at the rib-to-deck weld joint mainly focused

on the *root-deck* crack.

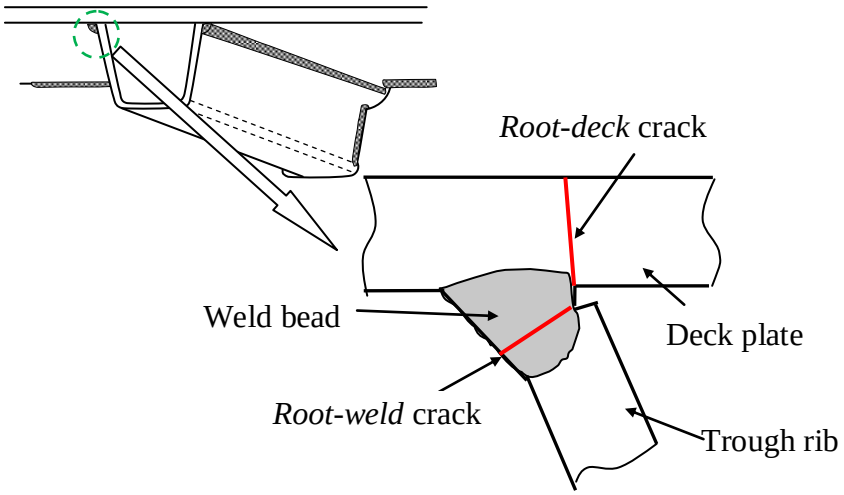

Fig.1.4 Fatigue cracks at rib-to-deck welded joint in orthotropic steel deck

As shown in **Fig. 1.5**, some *root-weld cracks* detected in actual orthotropic steel deck have a relatively long length. Moreover, the cracks suddenly change their propagation direction into the trough rib. The fatigue cracks initiated at the weld root and penetrated the weld bead. The through-thickness cracks propagated in the longitudinal direction along the weld bead, and then suddenly changed direction to the rib wall. The damage to the rib wall may decrease the stiffness of the orthotropic steel deck and cause a serious traffic disaster. However, unfortunately, the reason why the crack suddenly propagates into the trough rib is not clear.

Mori et al (2006) performed finite element stress analysis and fatigue test in order to clarify the cause of the *root-weld crack*. The influences of weld penetration depth and position of wheel load on the stress properties were investigated. Ya et al. (2009) pointed out that the main cause of a *root-weld crack* is an insufficient thickness of the weld throat, and increasing the throat thickness can prevent a *root-weld crack*. Asane et al. (2011) carried out the fatigue test on orthotropic steel deck models and detected a *root-weld crack* with 60~80 mm of length in the test. However, since the direction change of the crack did not occur in the experiment, the cause of the crack propagation changing direction was not addressed.

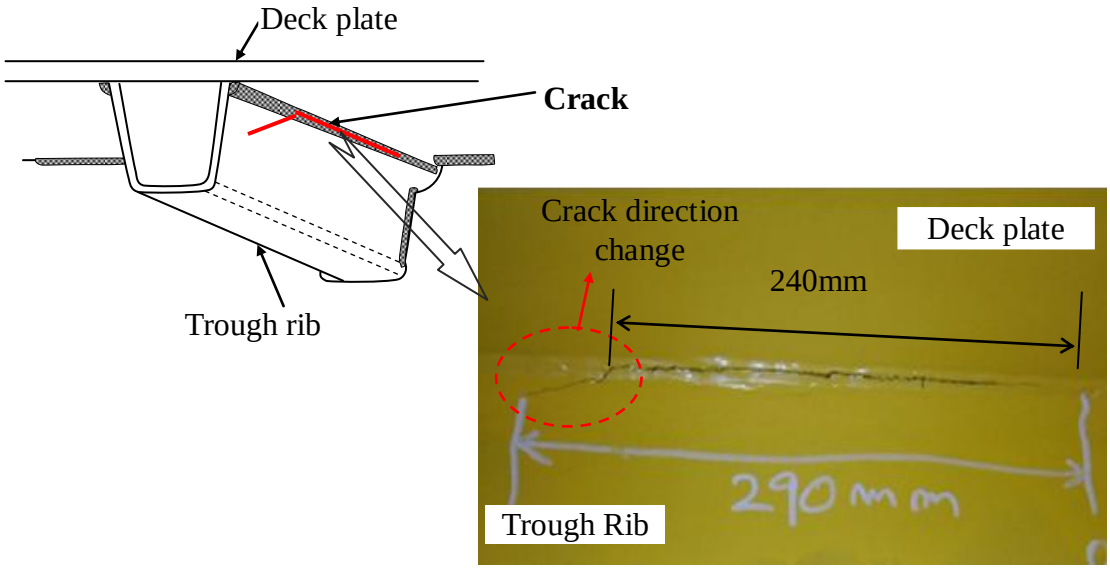

Fig 1.5 Direction change of through-thickness

1.2.4 Problems concerning through-thickness cracks under out-of-plane bending

Some research has been conducted on through-thickness cracks under out-of-plane bending. However, there are still significant issues to be further clarified. Some comments and discussions are as follows.

Firstly, the SIF distribution along the crack front is complicated by the stress gradient through the plate thickness direction and the crack closure at the compression side. The SIF distribution along the crack front can affect crack behavior in the next propagation. The previous studies conducted limited FEA with crack closure on the compressive side. However, they did not examine the crack closure state for the longer through-thickness crack, and they did not confirm either the effect of crack length and plate thickness on the crack closure or SIF distribution along crack front.

Secondly, previous studies established the equations for calculating SIF of through-thickness cracks under out-of-plane bending based on the assumption that the crack-front shape was straight. However, since the non-uniform SIF distribution along a crack front causes uneven crack growth, the crack front may not be a straight line. There are currently no experimental studies to investigate the crack-front shape of through-thickness cracks under out-of-plane bending.

Finally, a through-thickness crack at the weld bead sometimes changes its propagation direction into the rib wall. In order to assess whether it is potentially dangerous, it is essential to clarify the reason for the sudden change in propagation direction. Although there are several different fracture criteria for crack prediction, it is not clear which criteria is suitable for predicting this propagation behavior.

1.3 Research objectives

Based on discussions in the previous section, the purpose of this research is to identify crack propagation behavior of a long through-thickness crack under out-of-plane bending.

The objectives of the studies are as follow:

1) In order to investigate the effect of crack closure, plate thickness and crack length on SIF distribution along the crack front for a through-thickness crack under out-of-plane bending, an analytical study on cracked plates with various plate thicknesses and crack lengths was conducted considering the effect of crack closure.

2) In order to identify the crack propagation behavior of a through-thickness crack under out-of-plane bending, fatigue tests and FEA were carried out. The shape of crack front was investigated by fatigue tests. The SIF distribution along actual crack-front shape was examined by an FEA using actual crack-front shape. In addition, a correction factor that can express the SIF for a through-thickness crack under out-of-plane bending was proposed.

3) Using the established analytical model, examined the cause of sudden direction change in a through-thickness crack at the deck-to-rib welded joint in orthotropic steel decks.

1.4 Organization of this dissertation

Chapter 1 provides important background, previous studies, objectives and organization of the dissertation.

Chapter 2 addressed the SIF distribution along the crack front for a through-thickness crack subjected to out-of-plane bending, considering the crack closure on the compressive side. The effect of plate thickness and crack length on the crack closure was investigated by parametric analysis.

In Chapter 3, the crack-front shape of a through-thickness crack under out-of-plane bending was described. The simple calculation method for SIF of a through-thickness crack under out-of-bending was examined.

Chapter 4 dealt with the crack growth mechanism of the root-weld cracks in an orthotropic steel deck by FEA. Stress intensity factors for three deformation modes were estimated by the FEA and the displacement extrapolation method, and crack direction was predicted using the maximum energy release rate criteria.

Chapter 5 presented the summaries and conclusions of this study. Some suggestions for future study were also presented.

CHAPTER 2

STRESS INTENSITY FACTOR OF THROUGH-THICKNESS CRACK SUBJECTED TO OUT-OF-PLANE BENDING

2.1 Introduction

An important problem of out-of-plane bending is that the crack closure can occur on the compressive side. Alwar et al. (1983) performed 3-D FEA on a plate with a through-thickness crack subjected to out-of-plane bending. They confirmed that the SIF distribution along the crack front under out-of-plane bending is influenced by the crack closure. However, the analysis employed limited cases of crack length and plate thickness. To identify the crack propagation of relatively long through-thickness cracks, the influence of crack length and plate thickness on the SIF distribution should be examined.

In this chapter, 3-D FEA was carried out on plates with various crack lengths and plate thicknesses subjected to out-of-plane bending, and the SIF distribution along the crack front was investigated. In addition, the shape development of a through-thickness crack under out-of-plane bending was simulated by a crack propagation analysis.

2.2 Finite element model

Analyses were performed by using ABAQUS Ver.6.7. **Fig. 2.1** gives the FE model. Taking advantage of symmetry, a half model was created. In this analysis, the crack-front shape was assumed to be a straight line, as described in *Chapter 1*. Twenty-node quadratic brick elements were employed, and quarter point degenerated brick elements were used near the crack front. The size of one quarter point degenerate brick element was 0.1mm. The crack closure on the compressive side was simulated by assigning a contact condition between crack surfaces. The friction on the contact surfaces was ignored. SIF was calculated by the J-integral method. The SIF could be converted from J-integral which was evaluated from contour integrals. The nominal

stress at plate surface is 180 MPa.

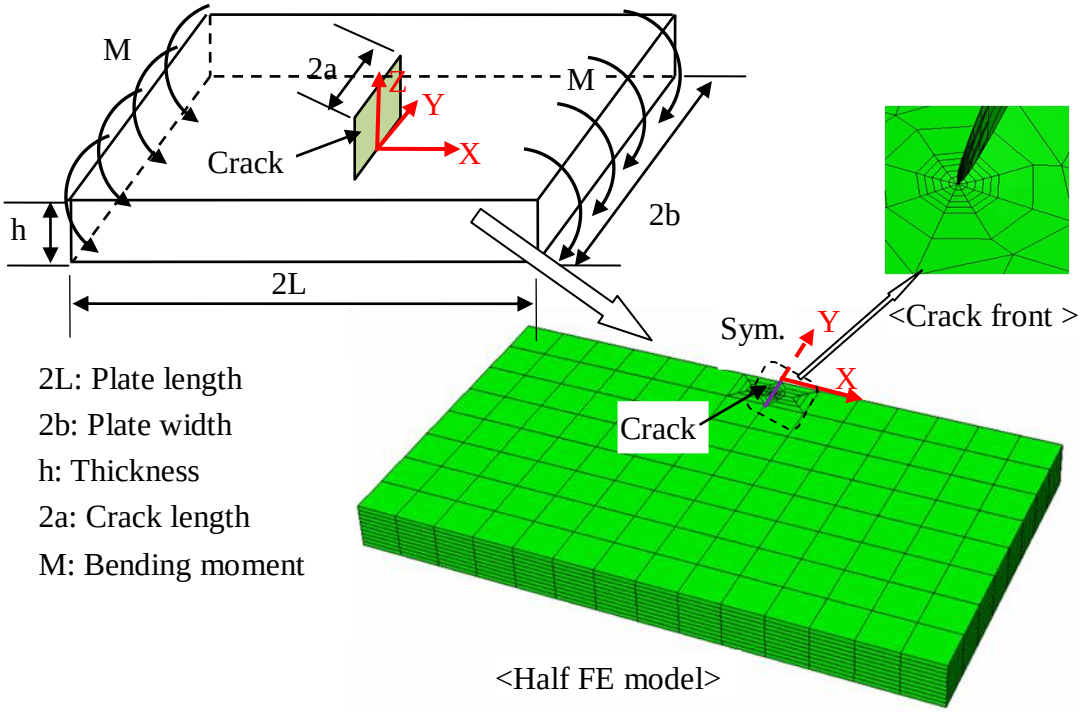

Fig.2.1 Finite element model

2.3 SIF distribution along the crack front

2.3.1 Effect of loading condition

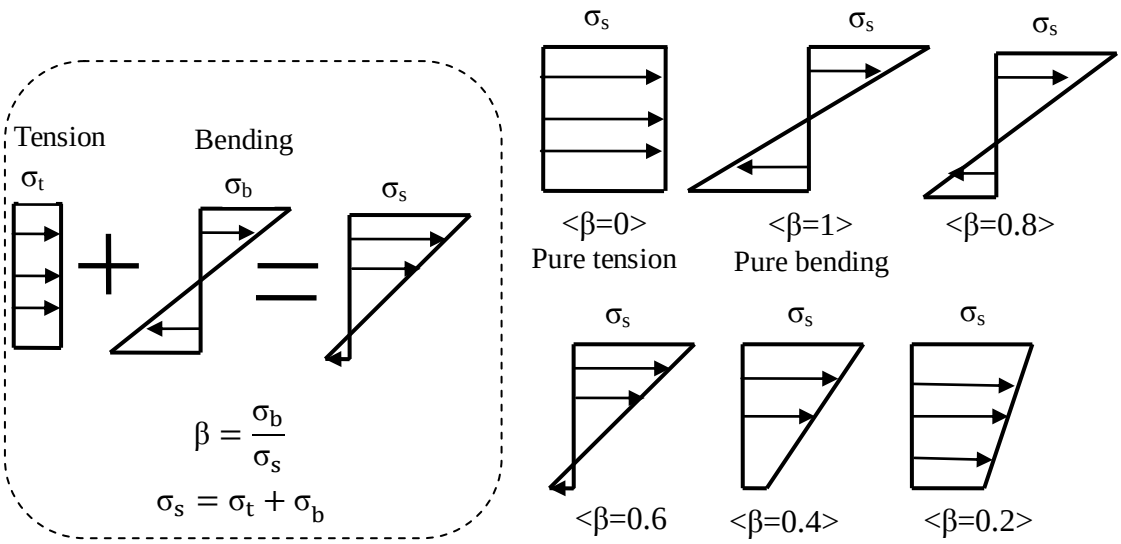

Fig. 2.2 Stress distribution in plate thickness direction

As the first step, the SIF distributions under tension and under bending were investigated. Various load cases with different stress ratios between bending and tension were applied. Here, bending stress ratio β is defined as shown in **Fig. 2.2**. The crack length ($2a$) and the plate thickness (h) were 50mm and 10mm, respectively. The plate width ($2b$) was 200mm. In order to make a comparison between the different loading conditions, the nominal stress σ_s at plate surface was same in all models, and the value was 180MPa.

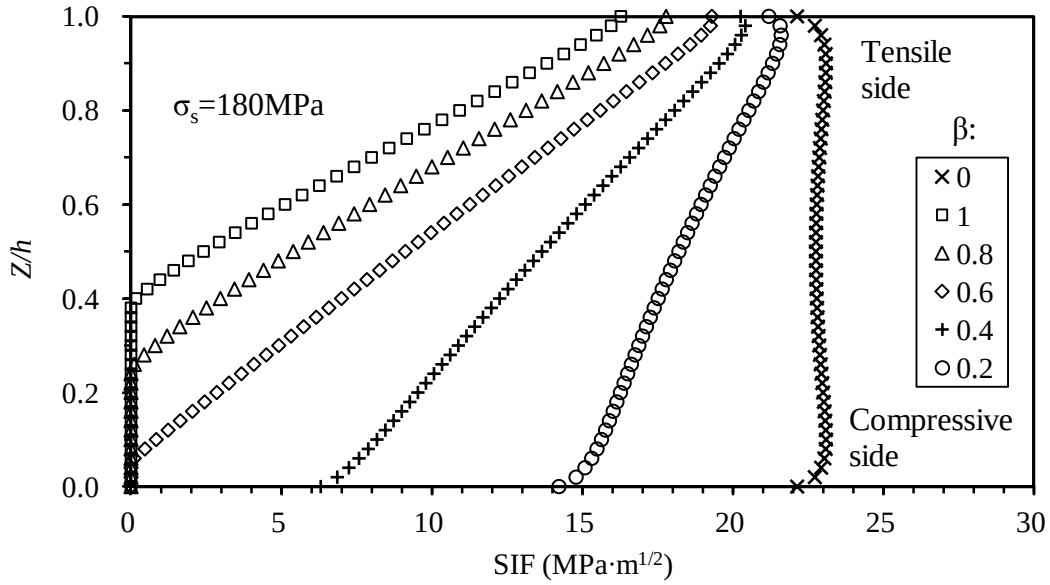

Fig. 2.3 SIF distribution along crack front under different bending stress ratios (β)

Fig.2.3 shows the SIF distribution along the crack front for each bending stress ratio (β). Under a pure tension condition (β=0), although the SIFs near both plate surfaces decrease slightly due to the effect of free surface, as a whole, the SIF distribution along the crack front is nearly uniform in the plate thickness direction. On the other hand, when the bending is introduced into the model, the SIF linearly decreases from the tensile side. Therefore, it can be said that the crack growth of a through-thickness crack under bending cannot be uniform in the plate thickness direction. Focusing on the maximum value of SIF for each bending stress ratio, although σ_s is same at the plate surface, the maximum SIF at the plate surface under pure tension (β=0) is about 1.36 times larger than that under pure bending (β=1). From the above results, it is obvious

that the SIF distribution along the crack front of the through-thickness crack depends on the bending stress ratio due to the stress gradient and the crack closure. Consequently, since the different crack growth rate is uneven in the plate thickness direction due to the non-uniform SIF distribution, the crack-front shape may not be a straight line under out-of-plane bending.

2.3.2 Effect of crack closure and crack length

As discussed in the previous section, the SIF distribution along the crack front is non-uniform under out-of-plane bending. Therefore, for the next step, the effect of crack closure on the SIF was investigated under out-of-plane bending. Two kinds of FE models were created: a model with the crack closure (hereafter 'closure') and a model without the crack closure (hereafter 'no-closure'). As mentioned above, the crack closure was simulated by assigning the contact condition on the crack surfaces. In the no-closure model, crack surfaces were set as free surfaces. The crack length ($2a$) was changed from 10mm to 110mm. The plate thickness (h) and the plate width ($2b$) were fixed as 20mm and 200mm, respectively. The nominal stress was set to be180MPa. Here, it must be pointed out that the load magnitude had no effect to the area of crack closure, which was proved by carrying out a preparatory analysis.

Fig. 2.4 shows the comparison of SIF variation between the no-closure model and the closure model. The SIF variation in the plate thickness direction is almost linear and is symmetric about the mid-plane of the plate, and this variation trend is consistent with the bending stress variation in the plate thickness direction. However, the SIF variation in the plate thickness direction for the closure models is non-symmetric. On the other hand, the SIFs with 5mm of crack length nearly coincide in both the closure and the no-closure models, but as the crack length increases, the SIF of the closure model becomes smaller than that of the no-closure model. **Fig. 2.5** shows the difference in the maximum SIF at the tensile plate surface between the no-closure and the closure model against the crack length normalized by the plate thickness. The figure reveals that the longer the crack length is, the larger the difference becomes. Therefore, to estimate the SIF of through-thickness cracks under out-of-plane bending, the crack closure should be considered in analytical models, especially for long through-thickness cracks.

Additionally, it is obvious that the opening region for shorter crack is closer to that for no closure case, and the height of crack closure region decreases with the crack length increasing, which is a possible reason why the difference between the closure and the no-closure models becomes larger with crack length increasing.

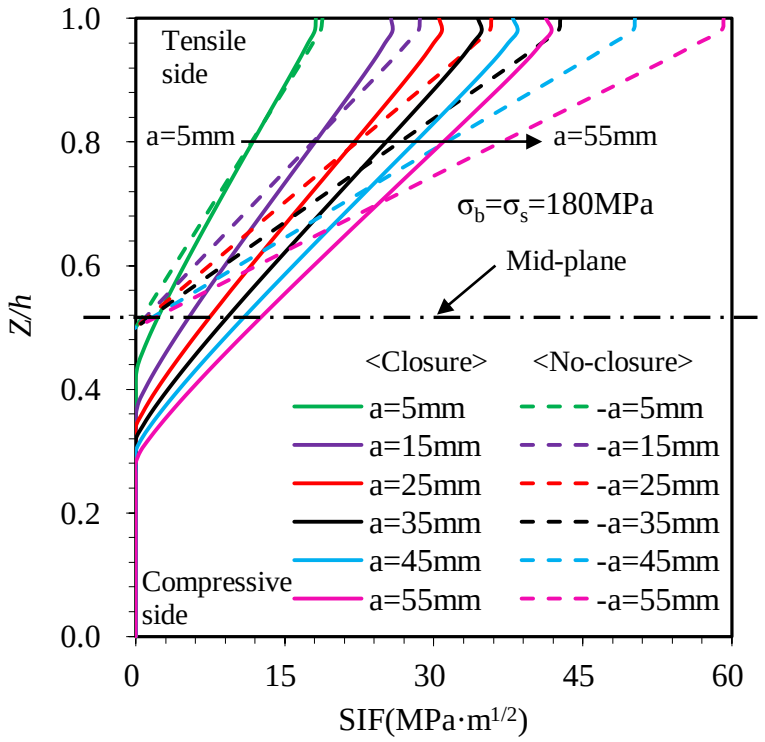

Fig. 2.4 Comparison of SIF distribution between no-closure and closure

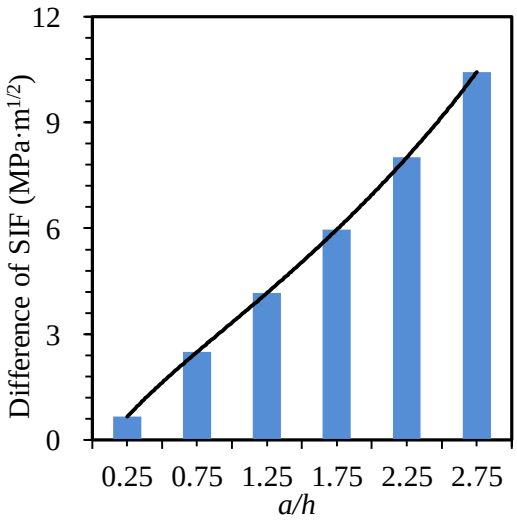

Fig. 2.5 Differences of the maximum SIF between no-closure and closure

2.3.3 Effect of plate thickness

Most of previous experimental studies were performed on relatively thin plates of less than 5mm. However, since such thin plates are rarely used in steel members, it is necessary to clarify the effect of plate thickness on the SIF. In this analysis, the plate thickness (h) was changed from 5mm to 40mm. The crack length ($2a$) and the plate width ($2b$) were fixed as 10mm and 200mm, respectively. The bending stress at the plate surface was 180MPa for all of models.

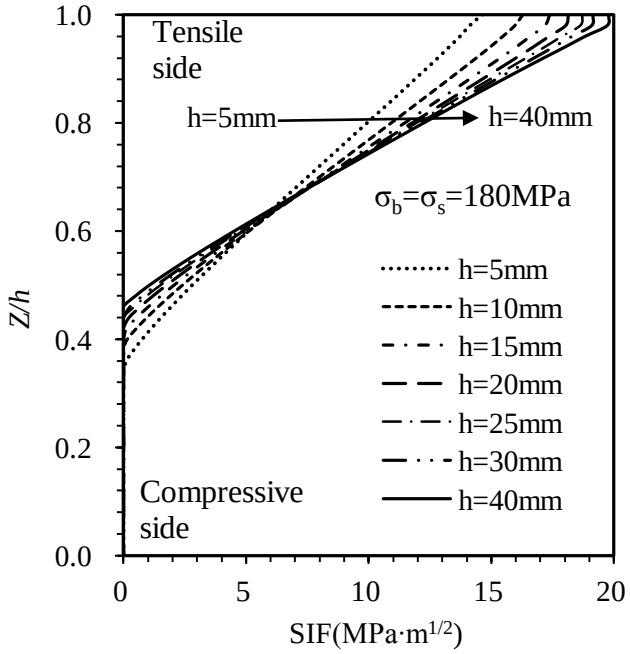

Fig. 2.6 SIF along crack front with different plate thickness

Fig. 2.6 shows the SIF distribution along the crack front with different plate thicknesses under bending. It indicates that the maximum SIF at the tensile plate surface increases as the plate becomes thicker. The SIF at the tensile plate surface for h=10mm thickness is about 10% larger than that for h=5mm. This means that the crack growth rate for thick plate is larger than that for thin plate under out-of-plane bending. However, most research on through-thickness cracks subjected to out-of-plane bending have been conducted with thin plates (less than 5mm), which are rarely used in steel bridges. The crack growth rate is considerably influenced by the stress gradient. Under the same nominal stress at the plate surface, the gradient of bending stress in the plate thickness

direction varies according to the plate thickness. Thus, plate thickness can be an influencing factor on the propagation behavior of through-thickness cracks under out-of-plane bending.

2.3.4 SIF Estimation of through-thickness crack

As mentioned in Chapter 1, Erdogan and Roberts (1965) proposed a simple equation (Eq. (1.3)) to estimate SIF for a through-thickness crack under out-of-plane bending by multiplying a correction factor α to Eq. (1.2) for a through-thickness crack under tension. The correction factor is the maximum SIF at plate surface normalized by Eq. (1.2). They also suggested 0.5 as the specific correction factor (α). According to previous sections, the SIF of the through-thickness crack was affected by crack length and plate thicknesses. In this section, the effect of plate thickness and crack length on the correction factor was investigated by parametric analysis.

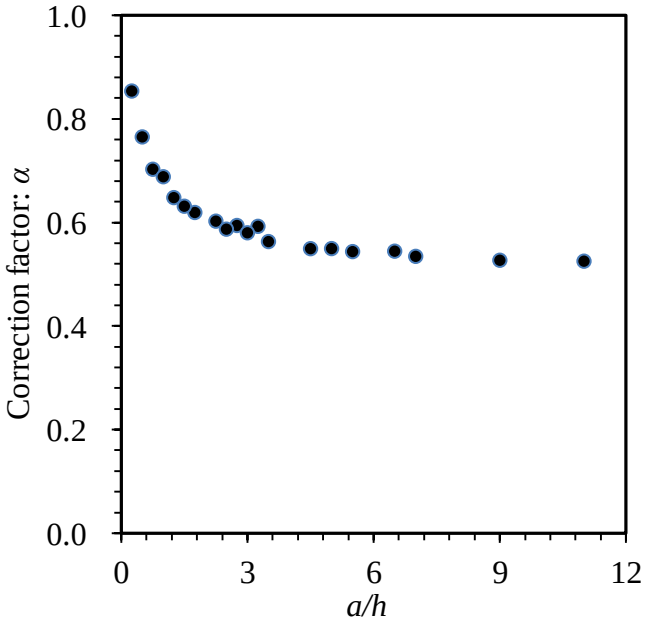

Fig. 2.7 Correction factor α VS a/h

Fig. 2.7 gives the relationship between the correction factor (α) and the ratio of crack length (a) and plate thickness (h). The crack length ($2a$) and plate thickness (h) employed for this analysis were 10~110mm and 5~30mm, respectively. The plate width was 200mm. Since the plate width is possible to influence the SIF, a preparatory

analysis was carried out to verify it. The analysis results revealed that the plate width had a relatively small effect on the SIF. Therefore, the effect of plate width on SIF was ignored. The correction factor is clearly influenced by the plate thickness and crack length. This leads to the conclusion that the correction factor increases with increasing plate thickness but decreases with increasing crack length. The correction factor increases rapidly, especially when the crack length is relatively small. Therefore, there are still questions that need further investigation in order to apply Eq. (1.3) to calculating SIF for various plate thicknesses and crack lengths. In order to improve the accuracy of the calculation, the effect of plate thickness and crack length on the correction factor should be considered.

2.3.5 Effect of crack front shape

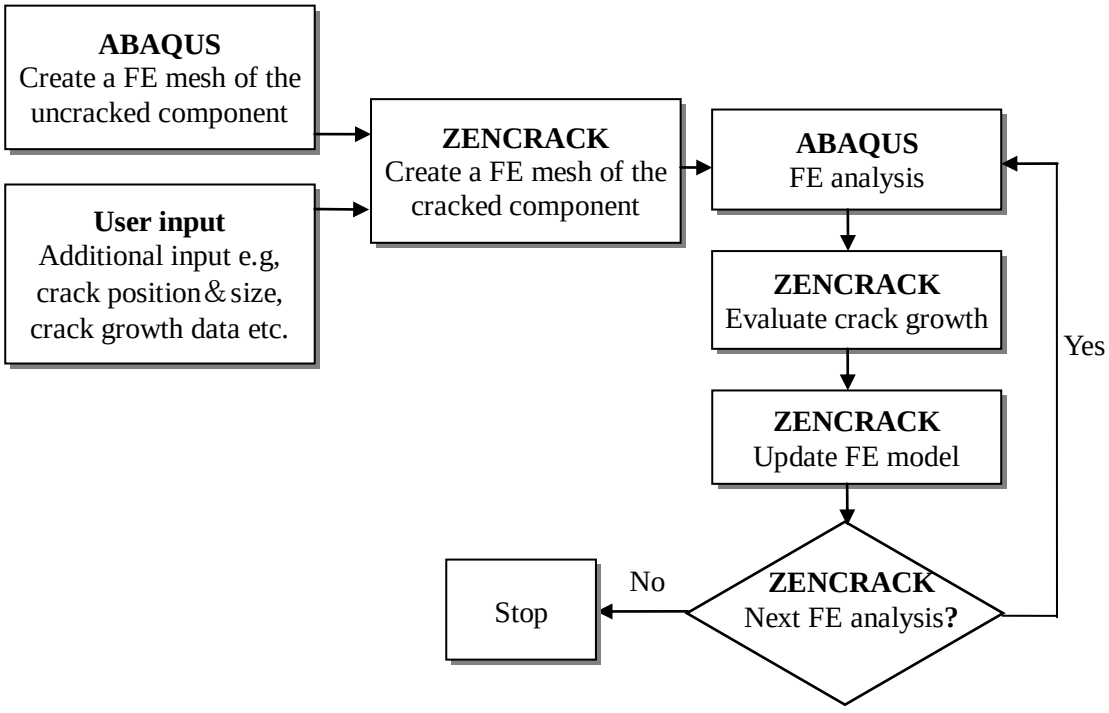

Fig.2.8 Flowchart of crack propagation analysis

From the previous sections, it was revealed that the SIF distribution along the crack front is non-uniform in the plate thickness direction under out-of-plane bending. The non-uniform distribution of SIF can affect the crack growth along the crack front. Therefore, the development of the crack front for through-thickness cracks under

out-of-plane bending was investigated by crack propagation analysis. Then, the effect of crack-front shape on SIF distribution was examined.

1) Crack propagation simulation

In this study, the crack propagation was simulated by ZENCRACK, which is commercial software for crack propagation analysis based on linear elastic fracture mechanics. **Fig. 2.8** shows the flow chart of crack propagation analysis. The geometries of the FE model used in the simulation analysis are: crack length (*a*) as 5mm, plate thickness (*h*) as 5mm, and plate width (*b*) as 100mm. The initial crack-front shape was a straight line. The crack closure on the compressive side was simulated by assigning a contact condition on crack surfaces. The friction on the contact surfaces was ignored. In this simulation, the crack propagation was based on the Paris' rule which made a relationship between crack growth rate and Mode-I SIF range.

2) Simulation results

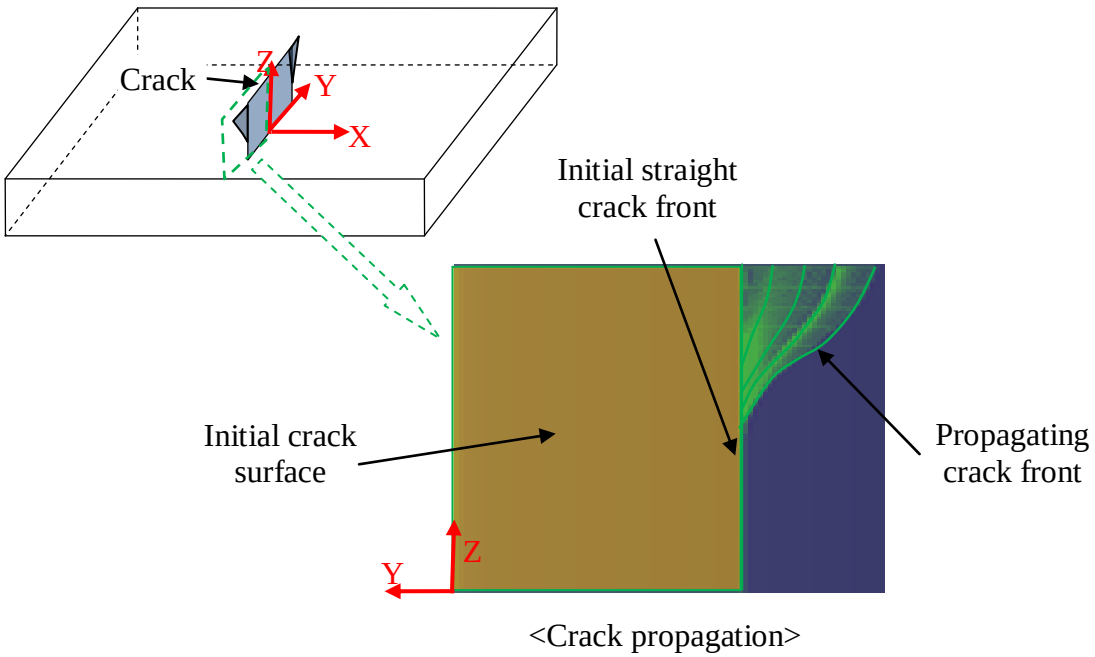

Fig. 2.9 Development of crack front shape

Fig. 2.9 shows the development of crack front shape. In this analysis, the stress ratio

was 0, and the nominal stress maximum at the plate surface is 180Mpa. It seems that although the initial crack front was given as a straight line, the crack growth rate changes across the plate thickness in the crack propagating stage. Therefore, the crack-front shape of the through-thickness crack is not straight line but curve across the plate thickness.

As the next step, the SIF distribution along the initial crack front and the propagating crack front was compared, as shown in **Fig. 2.10**. While the SIF is distributed linearly along the initial straight crack front on the tensile side, the SIF distribution along the propagating crack front behaves with non-linear variation. Besides, the maximum SIF at the plate tensile surface for the propagating crack front is smaller than that for the initial straight crack front. Therefore, it can be confirmed that the crack-front shape becomes a curve under out-of-plane bending due to non-uniform SIF distribution. In the next chapter, the crack-front shape will be investigated in detail by fatigue tests.

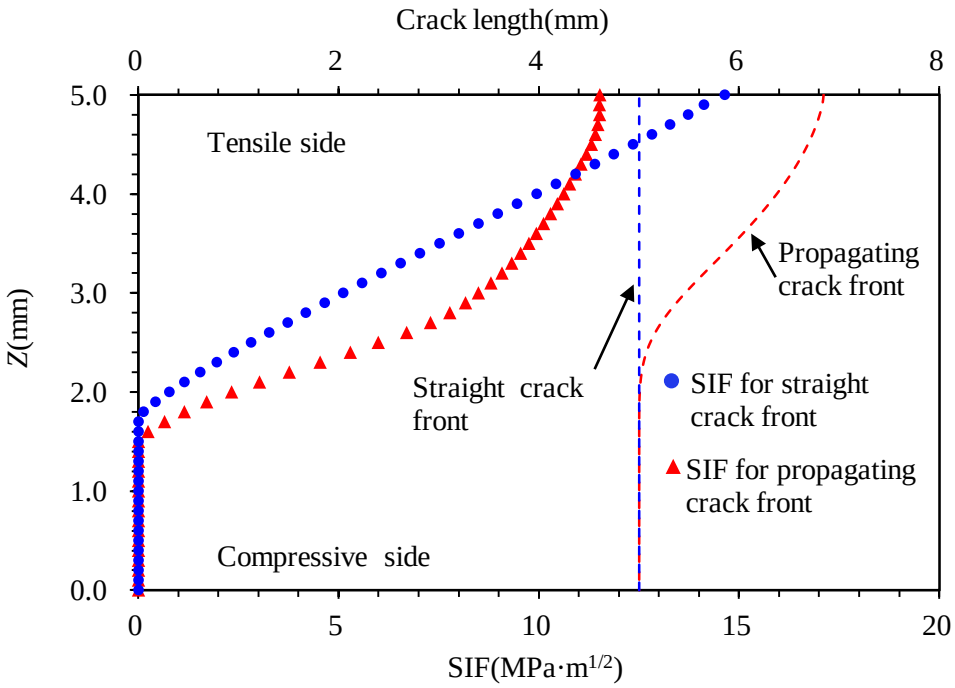

Fig. 2.10 SIF distribution along crack front

2.4 Conclusion

FEA on a through-thickness-cracked plate under out-of-plane bending was carried out. The results were as follows,

1) The SIF distribution along the crack front under in-plane tension was nearly uniform across the plate thickness, but SIF under bending changed due to the effect of the stress gradient and the crack closure on the compressive side. This indicates that the crack-front shape in the next propagation cannot maintain a straight line. In addition, the maximum SIF under pure tension was remarkably larger than that under pure bending. Therefore, to estimate the SIF, the effect of the load condition should be considered.

2) The SIF distribution for 5mm of crack length nearly coincides in both the closure and the no-closure models; however, as the crack length becomes longer, the difference in SIF becomes larger. Therefore, to estimate the SIF of through-thickness cracks under out-of-plane bending, the crack closure should be considered in analytical models, especially for long through-thickness cracks.

3) From the investigation on the effect of plate thickness, it can be seen that the maximum SIF at the tensile plate surface increases as the plate becomes thick.

4) From the crack propagation simulation, it was found that the straight initial crack front becomes curved in the next propagation due to the non-uniform SIF distribution in the plate thickness direction. The SIF distribution along the straight crack front is linear at the tensile side, but the SIF distribution along the curved crack front is not linear. Therefore, it can be confirmed that the crack-front shape affects SIF distribution.

CHAPTER 3

CRACK FRONT SHAPE AND STRESS INTENSITY FACTOR OF THROUGH-THICKNESS CRACK

3.1 Introduction

Limited research has been conducted on a through-thickness crack under out-of-plane bending. Erdogan and Roberts (1965) carried out a comparative investigation on the crack propagation behavior of a through-thickness crack under out-of-plane bending and proposed a simple method to calculate the SIF. Kanazawa and Machida (1974) theoretically investigated the SIF under the combination of tension and out-of-plane bending by assuming the equivalence of plastic zone size. In these studies, the crack-front shape was assumed as a straight line.

According to the crack propagation analysis in Chapter 2, due to the crack closure on compressive side, the crack-front shape can be changed in plate thickness direction under out-of-plane bending. Therefore, in this chapter, the crack-front shape of a through-thickness crack under out-of-plane bending was investigated by fatigue test, moreover, the SIF along the crack front was estimated by using FE model with an actual crack-front shape obtained by the fatigue test.

3.2 Fatigue test on cracked plate under out-of-plane bending

3.2.1 Test programs

The material properties of the hot rolled steel plate are shown in **Table 3.1**. The geometric configurations of the specimen are illustrated in **Fig. 3.1**. Four through-thickness notches of 8 mm in length and 0.2 mm in gap were introduced on the specimen edges as starters of fatigue crack. The plate is 15mm thick. Strain gauges were allocated at 35mm away from the notch tip on the both surfaces.

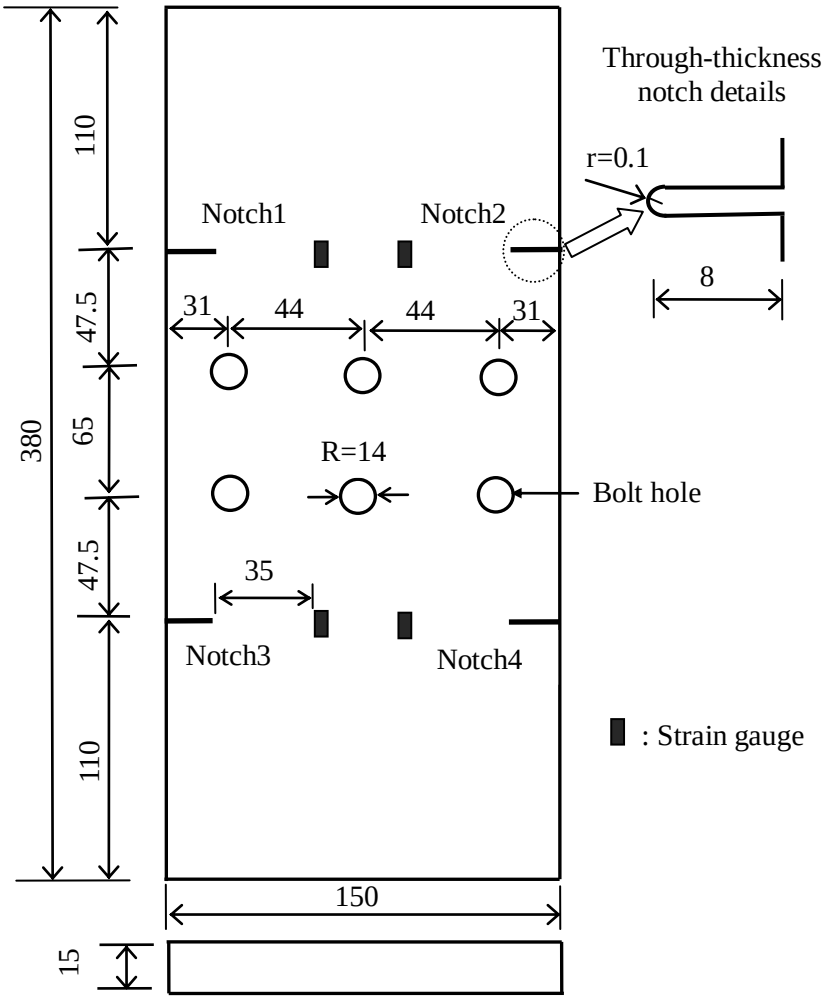

Fig.3.1 Geometry configurations of specimen (Unit: mm)

Table 3.1 Material properties of steel plate for experiment

Chemical composition (%)						Mechanical properties		
C	Si	Mn	P	S	Ni	Y.S(N/mm^2)	T.S(N/mm^2)	El
0.16	0.26	1.51	0.022	0.004	0.01	463	571	0.15

The test was performed with a servo-hydraulic fatigue testing machine. In order to introduce out-of-plane bending, the circular steel bars welded on end plates supported the two ends of the specimen, as shown in **Fig.3.2** and **Fig.3.3**, and the middle part of the specimen was connected to the fatigue testing machine by bolts. Through the comparison of the compressive surface stress and tensile plate surface stress, it found

that the effect of axial force caused by the friction between the circular steel bar and specimen was relatively small. Therefore, in this test, the influence of the friction was ignored. A sinusoidal waveform of displacement with constant amplitude was applied to the specimen. The loading frequency was 5.0 Hz. The nominal stress on the surface was calculated based on the strain measured by strain gauges. The test conditions are shown in **Table 2.2**. The stress ratios (R) were from -0.25 to -1.0. The amplitude of the sinusoidal wave displacement was about 2mm, and increased by small margins as the crack propagated. Crack length on the plate surface was monitored during the test. Additionally, in order to observe the shape of the crack front, beach marks were introduced by changing the load condition, as shown in **Table 2.2**.

Table 2.2 Test conditions

Load condition				Load condition for beach mark				Stress ratio (R)
Bending load(KN)		Surface bending stress (MPa)		Bending load(KN)		Surface bending surface (MPa)		
Max	Min	Max	Min	Max	Min	Max	Min	
19.2	-19.2	125	-125	9.6	-9.6	62	-62	- 1
30	0	0	-193	30	15	-97	-193	0
28	-21	136	-185	21	-14	92	-137	- 0.75
28	-14	92	-182	21	-10.5	70	-136	- 0.5
32	-8	52	-206	24	-6	40	-160	- 0.25

$R = \sigma_{min} / \sigma_{max}$

where,
σ_{min}: Minimum stress
σ_{max}: Maximum stress

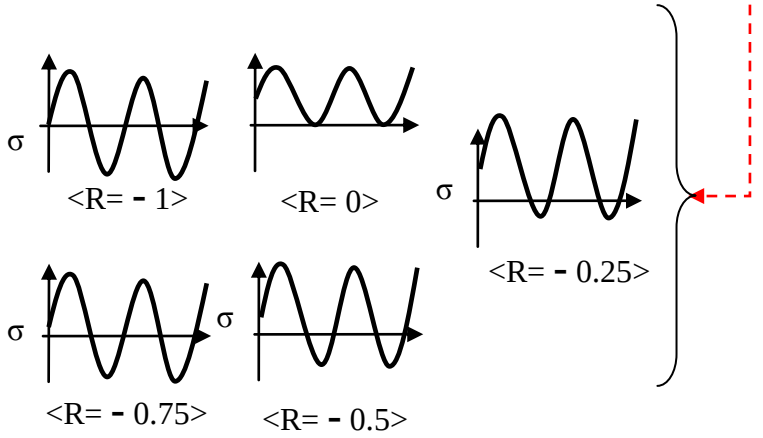

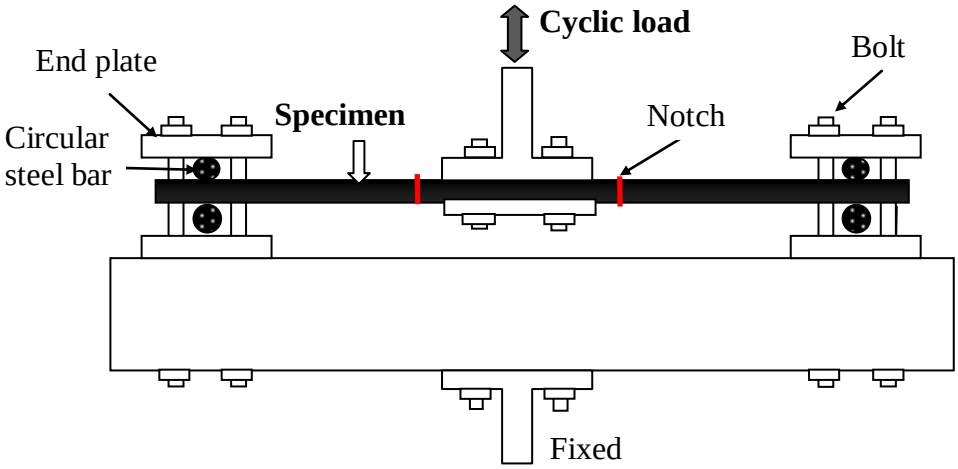

Fig. 3.2 Loading device

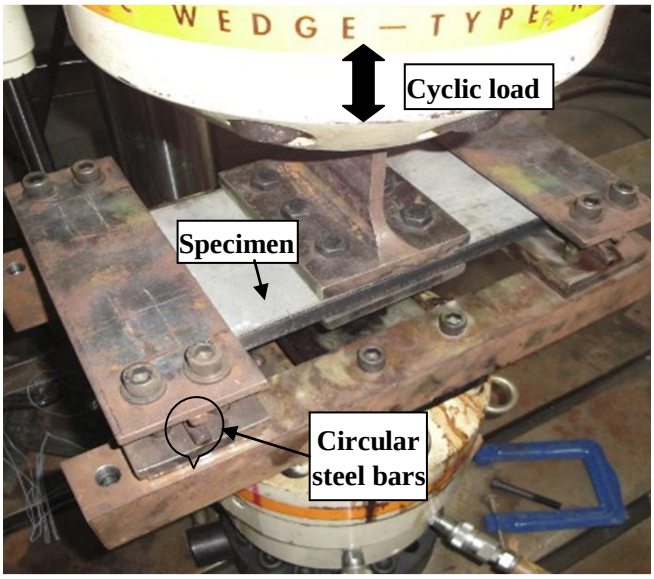

Fig. 3.3 Test setup

3.2.2 Fatigue test results

Fig. 3.4 shows the fracture surface for each stress ratio (R). At R=0, the fatigue crack has a quarter-ellipse shape which is the typical crack shape of a surface crack in tension. Excepting R=0, fatigue cracks were observed on both surfaces of the plate. However, as a whole, the crack shapes at R=-0.25, -0.5, and -0.75 are similar to that at R=0. On the other hand, at R=-1, the fatigue crack has a symmetrical V shape, which is a unique crack-front shape compared with the other stress ratios.

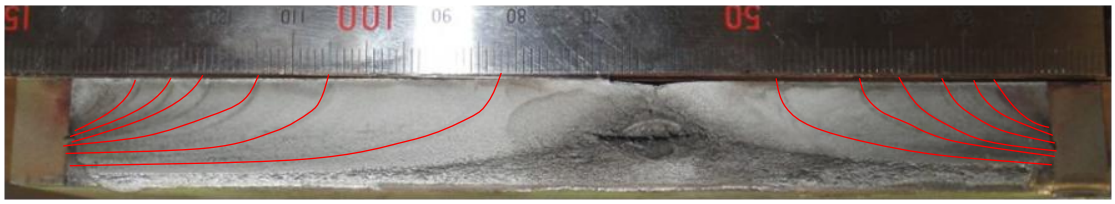

a) R=0

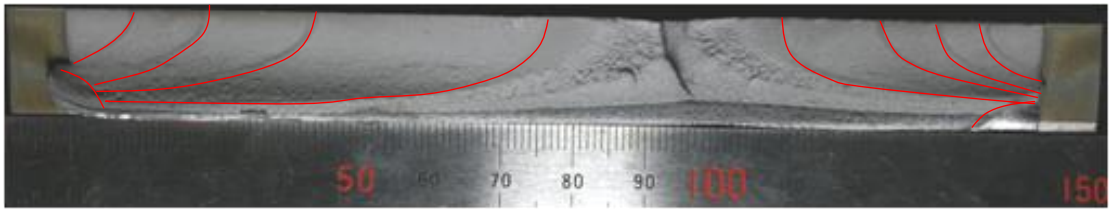

b) R=-0.25

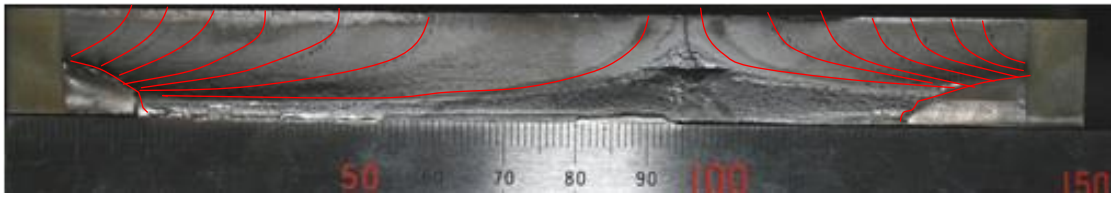

c) R=-0.5

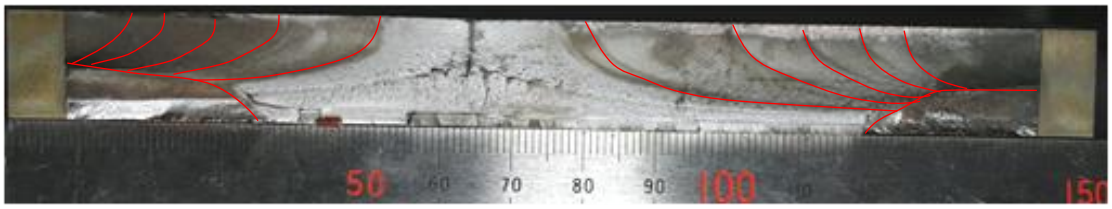

d) R=-0.75

e) R=-1

Fig. 3.4 Fracture surfaces

Additionally, it can be found that the cracks on the two sides of fracture surface are symmetric at R=-1, however, not symmetric at R=0, -0.25, -0.5, and -0.75, which may be related to the magnitude of the load. The maximum loads at R=0, -0.25, -0.5, and -0.75 are obviously larger than that at R=-1 as listed in **Table 2.2.** It is more difficult to control the balance of the specimen when larger load is applied, so the non-symmetric crack on the two sides of fracture surface is generated at R=0, -0.25, -0.5, and -0.75.

Fig. 3.5 shows the relationship between crack length and number of cycles in R=-1. The crack initiated from both surfaces of the plate where the maximum bending stress is generated, and penetrated to the center of the plate thickness. There was no crack propagation in the center of the plate thickness until the crack reached it. Once the crack started to penetrate to the middle of the plate thickness, as shown in **Fig. 3.5**, the crack growth curve at the center was almost parallel to that at the plate surface, which indicates that the crack growth rate at the center and at the plate surface is nearly identical.

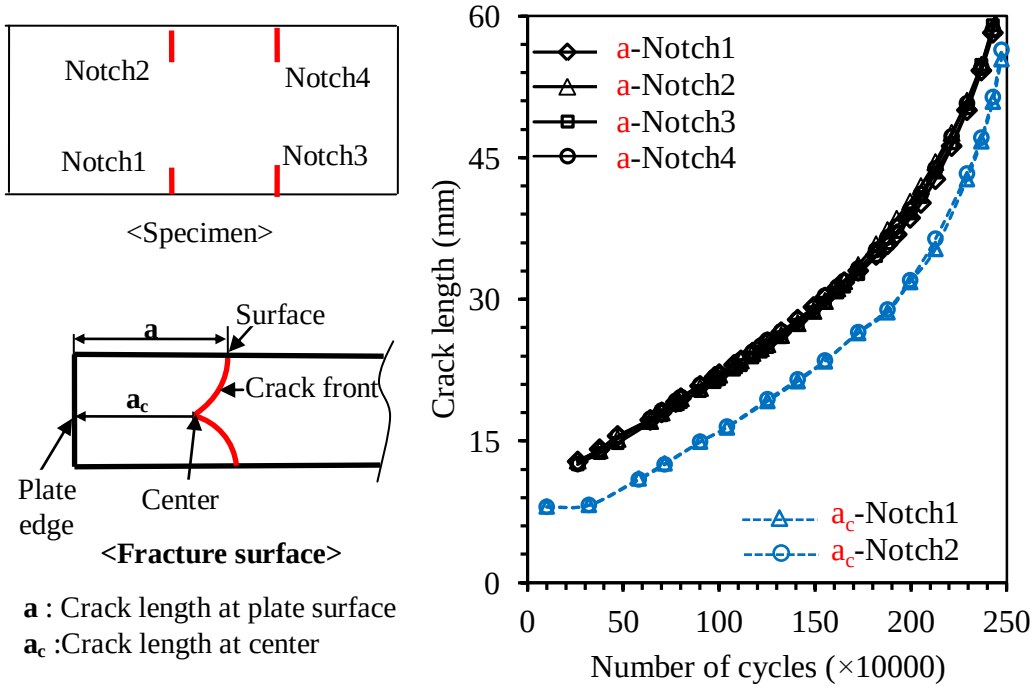

Fig. 3.5 Crack length vs. number of cycles (R=-1)

3.3 SIF estimation by FEA

According to fatigue test results on the cracked plate, at R=-1, the fatigue crack has a symmetrical V shape. This is a unique crack shape under out-of-plane bending. Therefore, the SIF distribution along the V-shaped crack front was calculated by FEA to identify the propagation behavior under out-of-plane bending

3.3.1 FE model

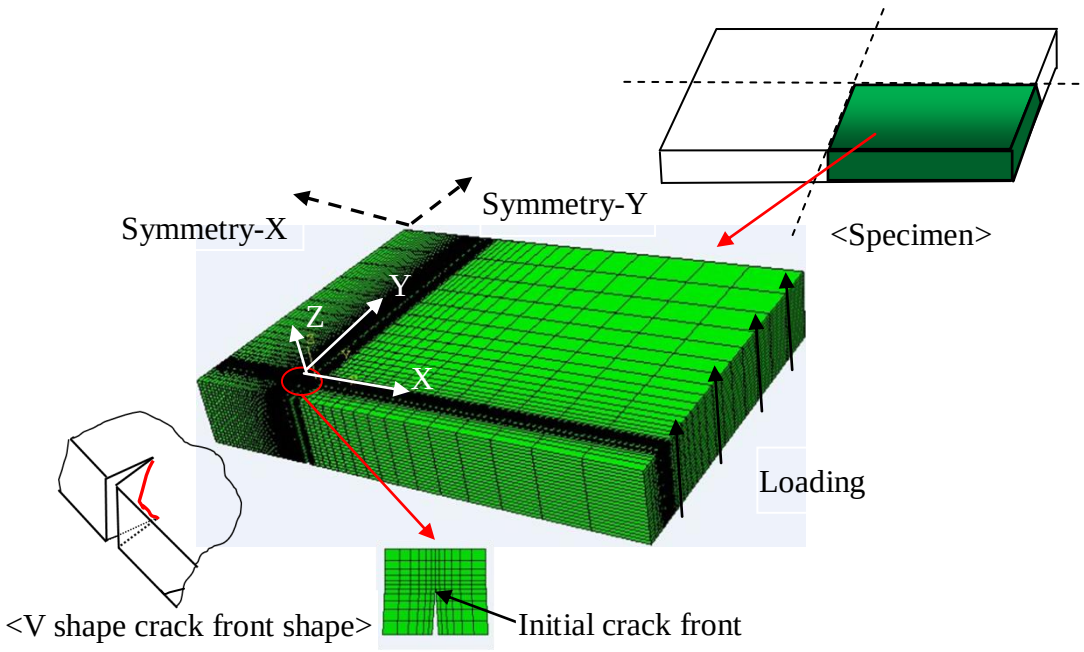

Fig. 3.6 FE model

Fig. 3.6 shows the analysis model and boundary conditions. Since both the model and the load are symmetrical in the X and Y directions, a quarter of the specimen with a through-thickness crack was modeled using 20-node solid elements. Uniform shear stress was applied to the model in the Z-direction. Young's modulus and Poisson's ratio are set to be 210GPa and 0.3, respectively. The minimum mesh size is 0.1 mm adjacent to the crack front. Reduced integration technique was used to calculate the element stiffness matrix, which has been confirmed to give good results in the case of plate bending. In order to consider the crack closure at the compressive side, a contact condition was assigned to two crack surfaces. The friction between two surfaces was

ignored. As an important factor in assessing the crack propagation behavior, Mode-I SIF was calculated by J-integral method (Owen et al., 1983; Courtin et al., 2005). From the fatigue test results on the cracked plate, the crack front had a symmetrical V shape under out-of-plane bending. This crack shape was applied to the analysis model.

3.3.2 SIF distribution along crack front

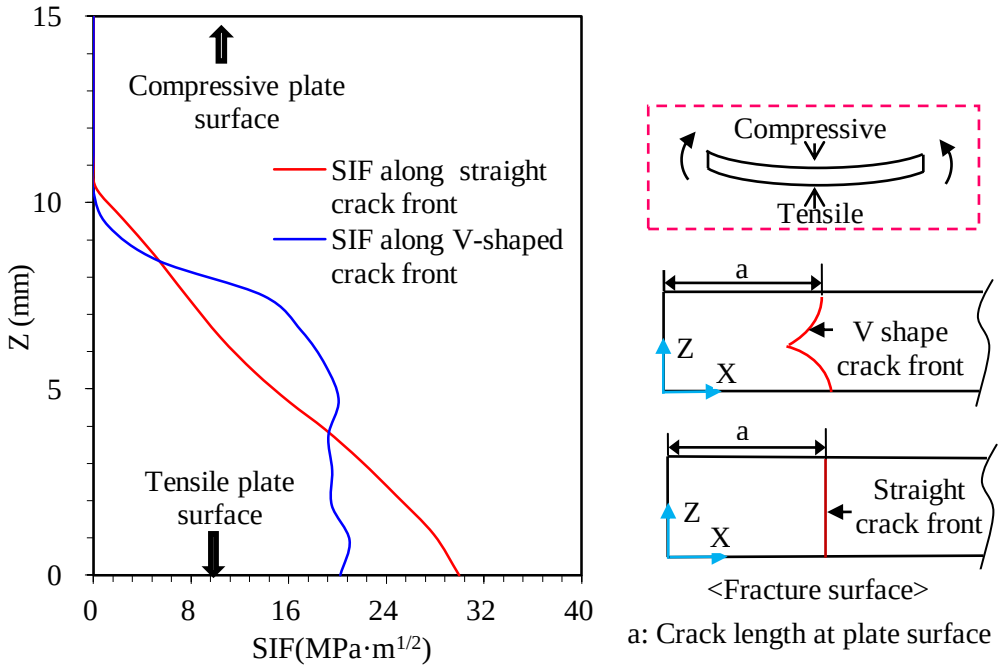

Fig. 3.7 SIF distribution along crack front under out-of-plane bending

Fig. 3.7 shows the SIF distributions along the V-shaped crack front. As a reference, SIF distribution for the straight crack front under the same load condition and crack length on the surface is also plotted. The SIF along the V-shaped crack front is roughly uniform in the tensile region and decreases as it approaches the compressive side, while the SIF along the straight crack front has almost linear distribution. Although the crack length on the surface is same, the SIF at the plate surface of the V-shaped crack front are smaller than that of the straight crack front. **Fig. 3.8** shows the SIF distributions along the crack front for different crack lengths. Regardless of crack length, SIFs in the tensile region are roughly uniform, and decline drastically around the interface of the tensile side and compressive side, and eventually become zero on the compressive side.

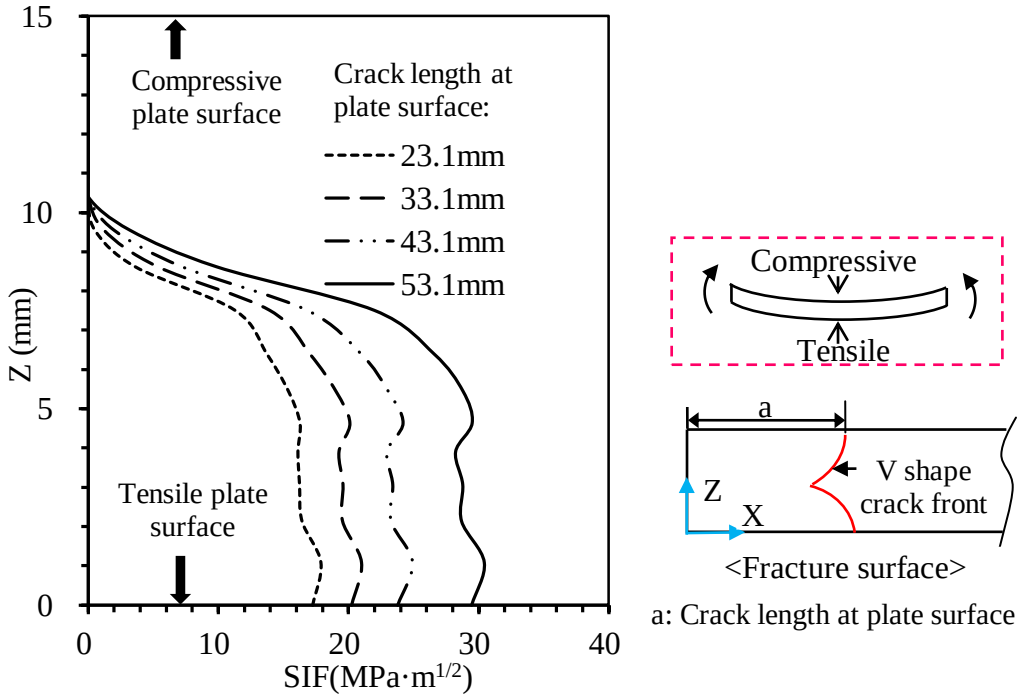

Fig. 3.8 SIF along V shape crack front with different crack lengths

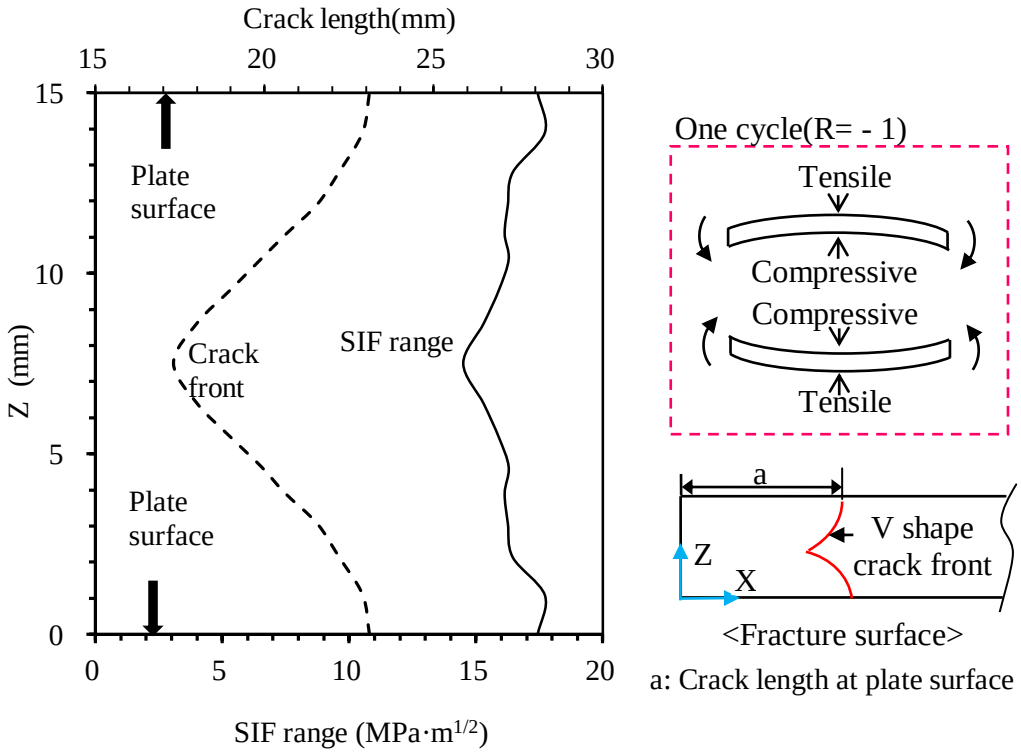

(a) Crack length at surface is 23.1mm

Fig. 3.9 SIF range along the curved crack front at R=-1

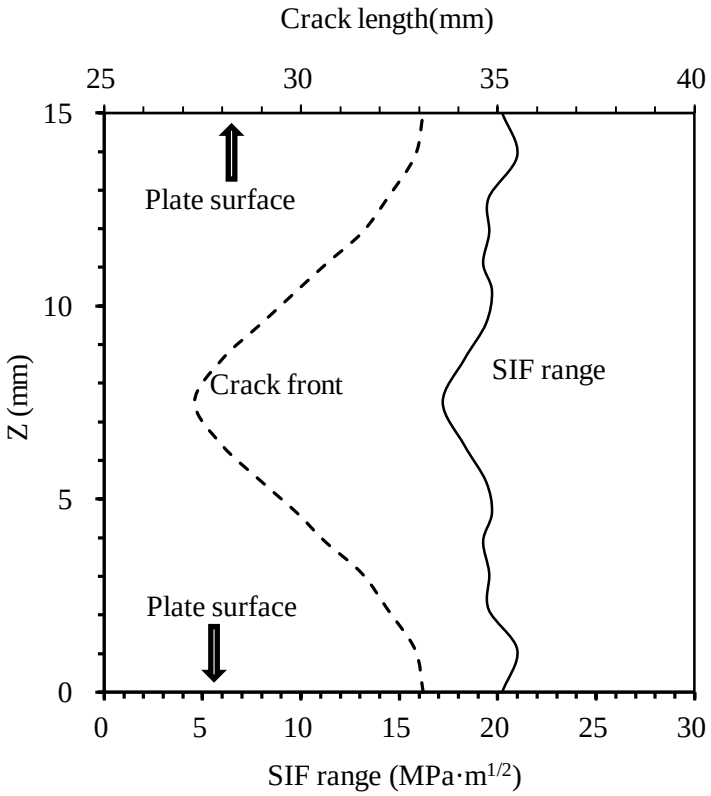

(b) Crack length at surface is 33.1mm

Fig. 3.9 SIF range along the curved crack front at R=-1(Continued)

3.3.3 SIF range under out-of-plane bending

Since the stress ratio is -1 in this test, the symmetric distribution must appear when inversed loading is applied. As examples, the SIF range (K_{max}-K_{min}) for two cases of crack length were presented in **Fig. 3.9**. The solid line indicates analysis results, and the dotted line is the crack-front shape through plate thickness. This leads to the conclusion that the SIF ranges for the different crack lengths stay approximately uniform through the plate thickness.

As described in Chapter 1 and 2, the stress intensity factor (K) for a through-thickness crack under tensile load is given as Eq. (1.2). In order to consider the effect of out-of-plane bending, previous researchers (Erdogan et al, 1965, Kanazawa et al, 1974) employed a correction factor α given in Eq. (1.3), which is the maximum SIF at plate surface normalizing by Eq. (1.2).

Erdogan and Roberts proposed 0.5 and Kanazawa and Machida proposed 0.45 as the correction factor under out-of-plane bending. These proposals, however, are based on the theoretical considerations of a straight crack front through plate thickness. According to the results in the previous sections, the crack front under out-of-plane bending is V shape. But the SIF range is almost constant through the plate thickness even though the crack front is V-shaped. Therefore, this research adopted the same concept to the existing method and applied a correction factor, shown in Eq. (1.3).

The average of the SIF range along the V-shaped crack front under out-of-plane bending was estimated, and the SIF ranges with crack growth were investigated to describe the crack propagation behavior. The ratio of the SIF range for out-of-plane bending ($\Delta K_{bending}$) and SIF range (ΔK) in tension calculated by Eq. (1.3) is determined as a correction factor under out-of-plane bending. In this study, the crack length *a* range is 15~54mm, and the half width *B* is 75mm.

Fig. 3.10 shows the relationship between the correction factor and normalized crack length. The correction factor slightly decreases with the increase of crack length. The range of correction factors is about 0.45~0.49 when normalized crack length is in the range of 1~3.5. Because the correction factors have a small variation range with the crack length changes, the mean value can be applied to calculate the SIF in a simple way. The mean value of the correction factor is 0.465, which is close to the values suggested in the previous study.

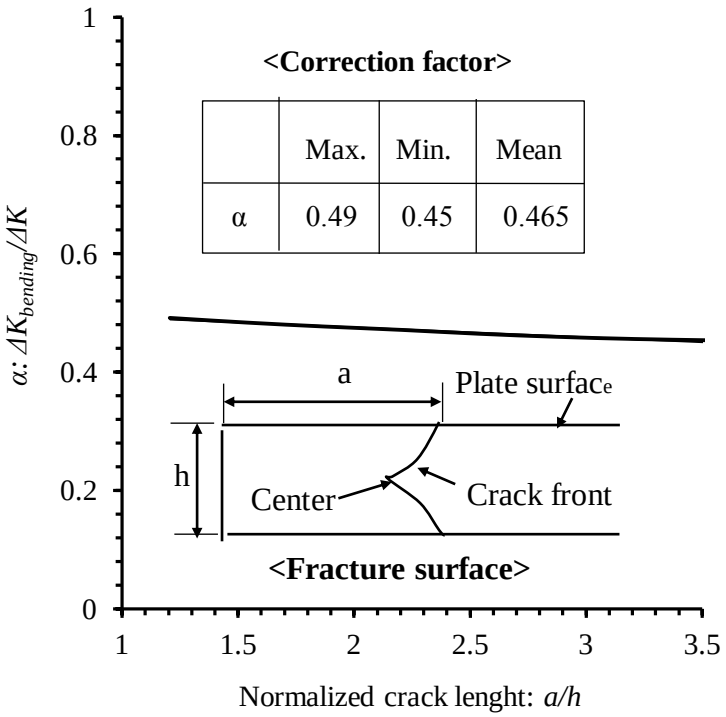

Fig. 3.10 Correction factor (*a* is crack length and *h* is plate thickness)

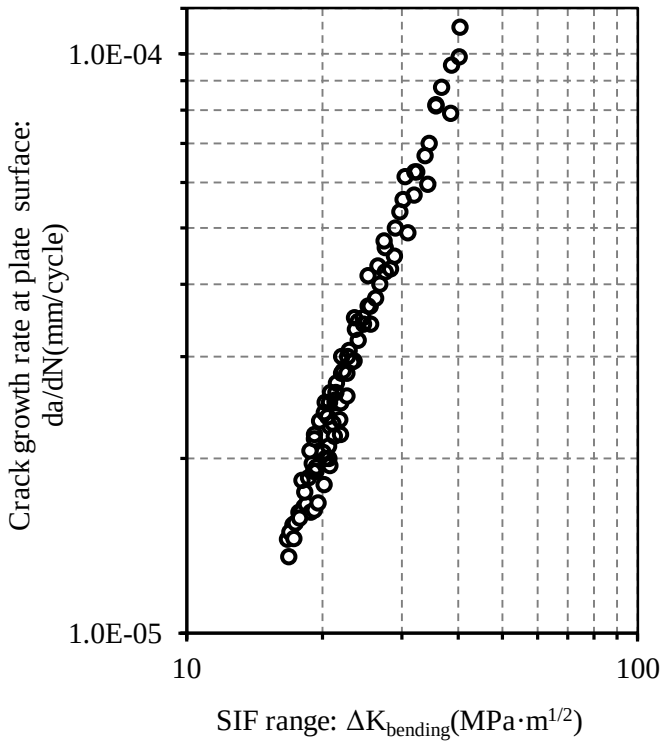

Fig. 3.11 Relationship between crack growth rate and SIF range

According to the SIF range calculated from FEA, the $da/dN - \Delta K_{bending}$ relationship was established. **Fig. 3.11** shows the results. All the data falls within a narrow band. Therefore, the crack propagation of the through-thickness crack under out-of-plane bending can be identified successfully by the proposed method above.

3.3.4 Crack propagation prediction

In order to verify availability of the proposed correction factor, the crack propagation was estimated using this factor based on Paris' law.

Calculation procedures of propagation life were carried out based on Paris' law:

$$dN = \frac{da}{C(\Delta K_{bending})^m} \rightarrow \int_0^N dN = \int_{a_i}^{a_f} \frac{da}{C(\Delta K_{bending})^m} \qquad (3.1)$$

The SIF range is simply expressed:

$$\Delta K_{bending} = \alpha \Delta\sigma \sqrt{\pi a} \cdot \sqrt{\frac{2B}{\pi a} tan \frac{\pi a}{2B}} \qquad (3.2)$$

where $\Delta\sigma$ is the stress range at surface, and a is the crack length at plate surface.

Thus, the number of cycles for one increment is determined as follows:

$$\int_0^{N_i} dN = \frac{1}{C} \int_{a_i}^{a_{i+1}} \frac{da}{(\alpha \Delta\sigma \sqrt{\pi a} \cdot \sqrt{\frac{2B}{\pi a} tan \frac{\pi a}{2B}})^m} \qquad (3.3)$$

And the total life is calculated as follows:

$$N = \sum_{j=1}^{n} N_j = \sum_{j=1}^{n} \frac{\Delta a}{C(\Delta K_{bending})_j^m} \qquad (3.4)$$

where, C is 1.6×10^{-11} and m is 2.25.

Fig. 3.12 plots the relationship between crack length at the plate surface, and the number of cycles obtained by experimental and numerical estimation. The results of the experimental and the numerical estimation agree well.

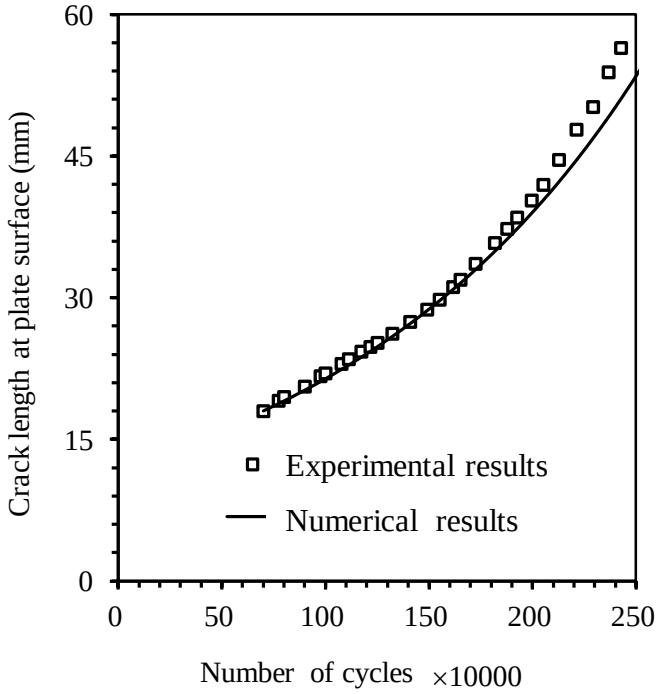

Fig. 3.12 Crack propagation prediction and experiment results

3.3.5 Effect of Mode-III loading

In the sections above, the evaluation of the SIF is mainly focused on Mode-I loading. However, considering the test loading condition, the specimen can be subjected to shear and out-of-plane bending at the same time. Therefore, the crack mode may fall under a mixed loading mode—Mode-I and Mode-III. In this section, the contribution of Mode III loading to the crack propagation is investigated.

It is evident that Mode-I loading due to out-of-plane bending plays a major role in crack propagation, but a branch crack on the base of the main crack can propagate due to Mode-III loading, as illustrated in **Fig. 3.13**. The Mode-III load can produce a twist effect, which causes the crack surface to curve (Pook et al., 1985). Generally, the crack surface is flat in a pure mode-I crack; however, the crack surface under mixed

mode-I/III loading is typically non-planar (Liu, 2004). As in **Fig. 3.14**, the crack surface is not completely flat due to the effect of Mode-III loading, which can influence the crack direction, especially in the center thickness.

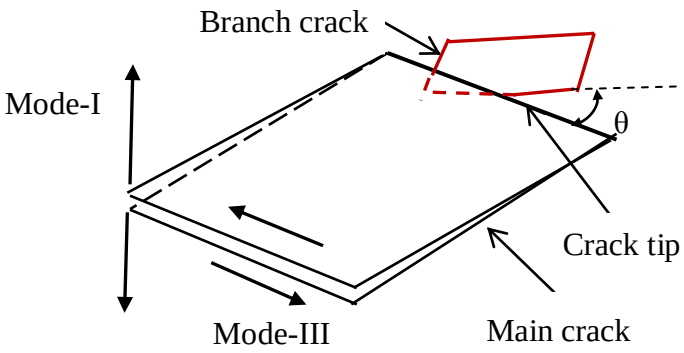

Fig. 3.13 Branch crack at main tip

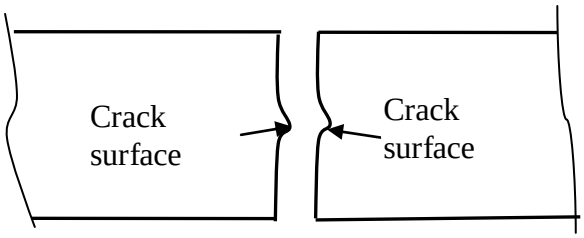

Fig. 3.14 Lateral view of fracture surfaces

In order to ascertain the influence of Mode-III loading, the Mode-III SIF (K_{III}) was investigated by FEA. The V-shaped crack was introduced into the analysis model, and SIF distribution along the crack front was analyzed. Here, the Mode-III SIF was calculated by displacement extrapolation method. As a reference, K_{III} distribution along the straight crack front under the same load is also plotted in **Figs. 3.15** and **3.16**. As examples, the distributions for 23.1mm and 33.1mm of crack length are represented. The SIF distribution along the straight crack front is nearly uniform, and the SIFs around the middle of plate thickness are a little larger than the SIF around plate surfaces. However, the SIF distribution along the V-shaped crack front is non-uniform. The SIFs increase as the crack propagates from the two surfaces into the middle of plate thickness. Moreover, the SIFs increase slightly near plate surfaces, and increase drastically near the plate center. An important point to note is that K_{III} values for the V-shaped crack front are smaller than those for the straight crack front near the plate surfaces, but the

reverse happens in the plate center.

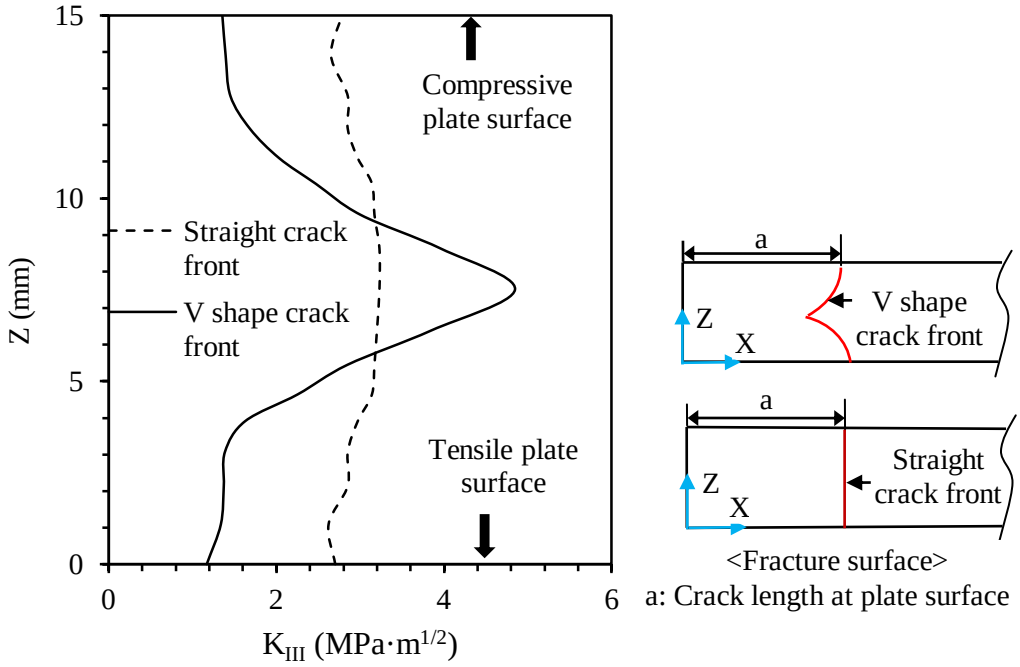

Fig. 3.15 Mode-III SIF for crack length at plate surface equal to 23.1mm

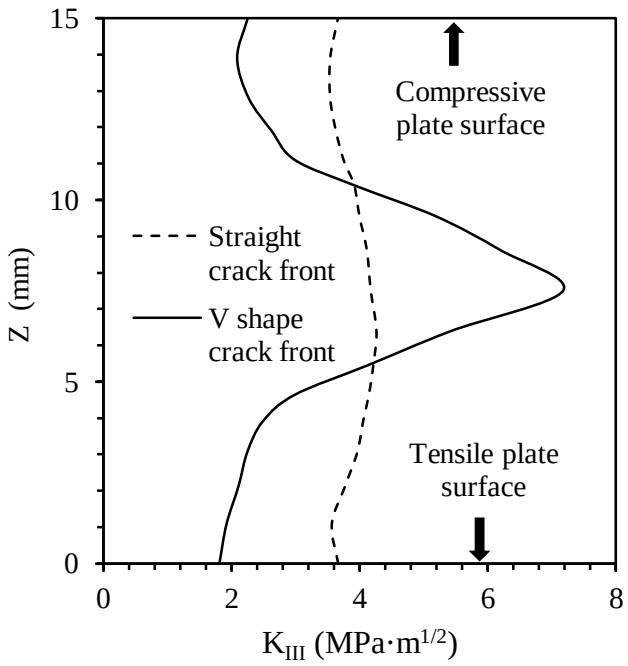

Fig. 3.16 Mode-III SIF for crack length at plate surface equal to 33.1mm

K_{III} along the V-shaped crack front with different crack lengths are given in **Fig. 3.17**. Although the SIFs adjacent to the compressive surface of the plate are a little larger than

that near tensile surface of plate, the SIF distribution along crack front is nearly symmetric to that in the middle of plate. Mode-III SIFs along the V-shaped crack front increase as the crack propagates from the two plate surfaces to the middle of plate thickness. The SIF near the middle of plate is larger than that near the two plate surfaces.

Based on the strain energy density theory (Shi, 1974), the combined SIF of Mode I/III can be expressed:

$$K_{com} = \sqrt{K_I^2 + \frac{1}{1-2\mu} K_{III}^2} \qquad (3.5)$$

where, μ is Poisson`s ratio, K_{com} is combined SIF of Mode I/III, K_I is Mode-I SIF, and K_{III} is Mode-III SIF.

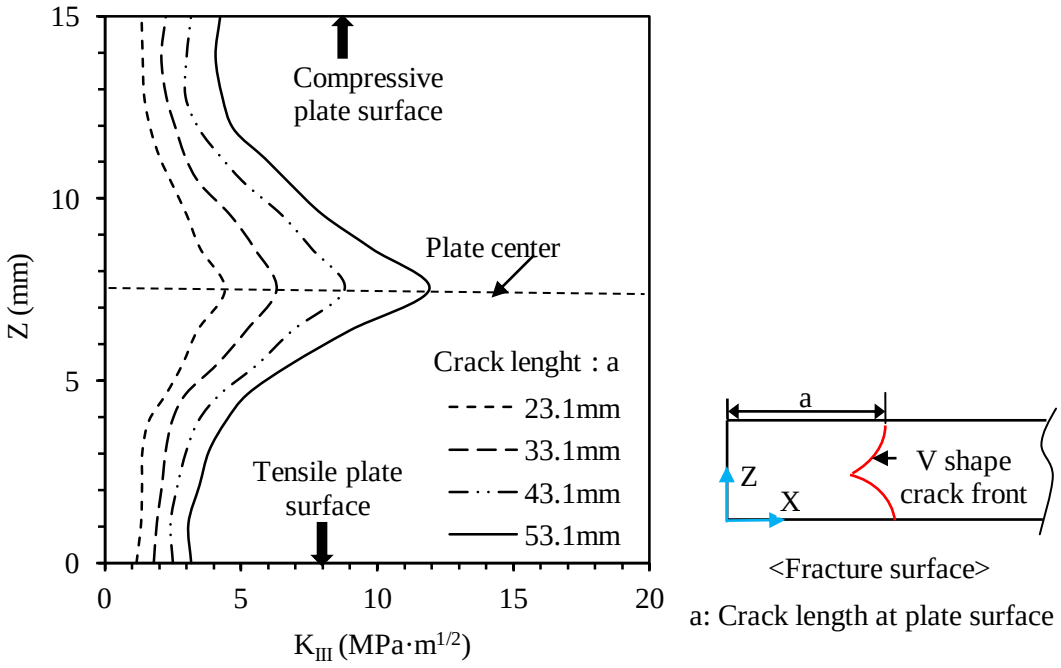

Fig. 3.17 Mode-III SIF along V shape crack front with different crack lengths

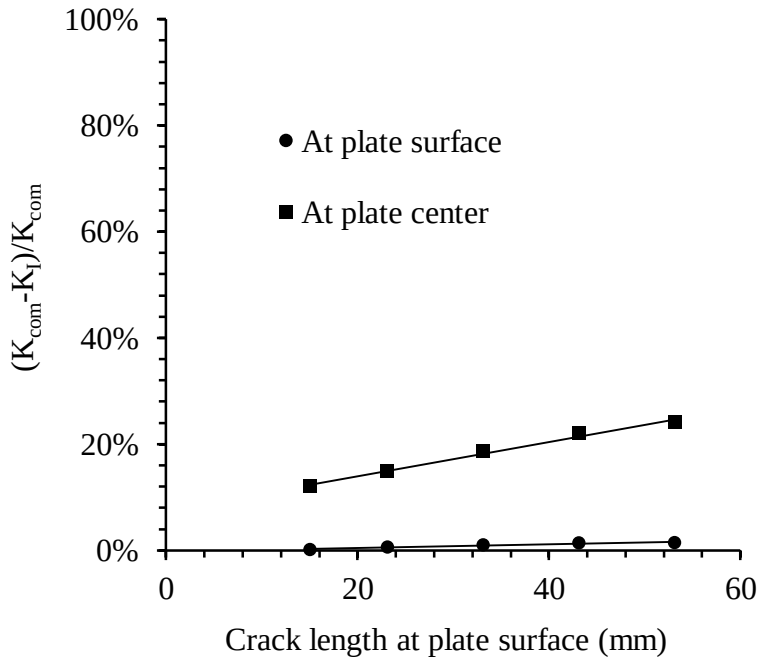

Fig. 3.18 A comparison between combined SIF of Mode-I/III and pure Mode-I

Fig. 3.18 describes the comparison between the combined SIF of Mode I/III and the pure Mode-I SIF with different crack lengths at the plate surface. The vertical axis refers to that the difference between combined SIF of Mode-I/III and Mode-I SIF. The combined SIF of Mode-I/III appears to be basically equal to the Mode-I SIF near the plate surface, which indicates that the Mode-III loading has only a small influence on crack growth. There are some small differences between the mixed Mode-I/III SIF and the pure Mode-I SIF at the plate center. However, the effect of the Mode-III load on crack growth at the plate center is relatively small. Therefore, it is concluded that the crack propagation depends mainly on Mode-I loading in this test, and that the contribution of Mode-III loading to crack propagation is negligible.

3.4 Conclusions

Experimental studies and numerical analysis on fatigue crack propagation of a through-thickness crack subjected to out-of-plane bending were performed. The main conclusions can be drawn as follows:

1) In R=-1, the fatigue crack has a symmetrical V shape, which is a unique

crack-front shape compared to the other stress ratios. Regardless of the crack length, SIFs in the tensile region are roughly uniform, decline drastically around the interface of the tensile side and compressive side, and eventually become zero in the compressive side. SIFs along the V-shaped crack front are roughly uniform at the tensile side, and the SIF range along the crack front is nearly uniform.

2) Based on the test results, a correction factor was proposed to express the SIF for a through-thickness crack under out-of-plane bending. Because the correction factors have a small range of variation across changing crack length, the mean value can be applied to calculate the SIF in a simple way. The mean value of the correction factor is 0.465, which is close to the values suggested in previous studies.

3) Mode-III SIFs along the V-shaped crack front increase as the crack propagates from the plate surface to the middle of plate thickness. The SIF near the plate center is much larger than that near the two plate surfaces. Through the comparison between the Mode-I SIF and combined Mode-I/III SIF, the effect from Mode-III loading on crack propagation is negligible in this test.

CHAPTER 4

PROPAGATION BEHAVIOR OF THROUGH-THICKNESS CRACK AT RIB-TO-DECK WELDED JOINTS

4.1 Introduction

Many types of fatigue cracks have been found in orthotropic steel deck plates (JSSC, 1995; JRA, 2002; Miki et al., 2006; Mori et al., 2006; Ya et al., 2011). Among them, the through-thickness crack at a rib-to-deck joint shown in **Fig. 4.1** is generated by out-of-plane bending of the deck plate and the trough rib. This fatigue crack initiated at the weld root between the rib and the deck plate, penetrated along the weld bead, and then suddenly changed the direction to the trough rib.

In chapter 3, an analysis model was established to identify the SIF distribution of the through-thickness crack under out-of-plane bending. In this chapter, by using this analysis model, the direction change of the through-thickness crack in an orthotropic steel deck was examined by the SIF.

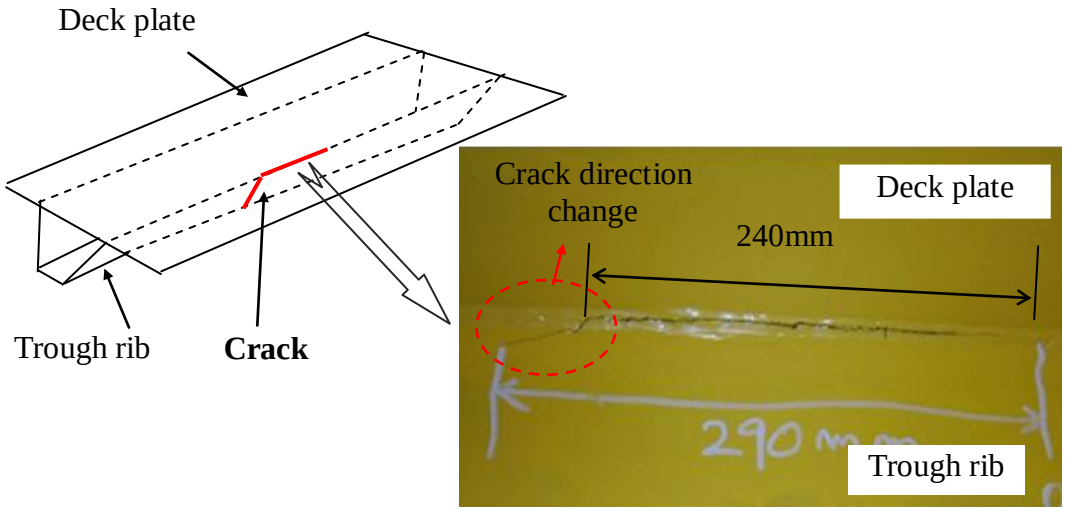

Fig. 4.1 Through-thickness crack at rib-to-deck welded joint

By using FEA, the SIF of the through-thickness crack was estimated by the displacement extrapolation method. Then, based on the maximum energy release rate criterion, the equivalent stress intensity factor and the crack direction were evaluated. Finally, the crack growth mechanism and the cause of the crack at the rib-to-deck welded joint changing its direction into the trough rib are both discussed.

4.2 Analysis model

4.2.1 FE model

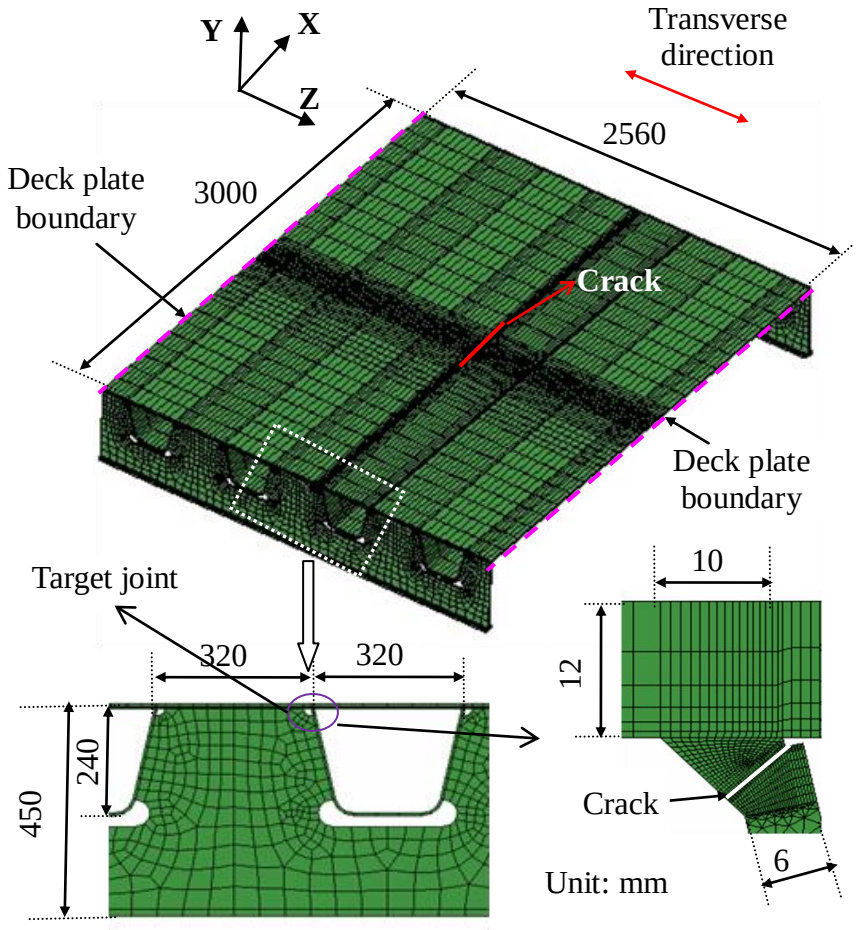

Fig. 4.2 FE model

In order to calculate the SIF of the through-thickness crack at the rib-to-deck joint, a finite element model of an orthodtropic deck was created with 8-node solid elements, as shown in **Fig. 4.2**. The minimum element size near the crack front was 0.2×0.2×0.2mm.

Young's modulus (*E*) and Poisson's ratio(ν) were set to be 210 GPa and 0.3, respectively. The interval of floor beams was 3,000mm, and the interval of longitudinal ribs was 640mm. Thickness of the deck plate was 12mm, and the thickness of the trough rib was 6mm. Weld penetration of the fillet weld between the deck plate and the rib was 75% of the trough rib thickness.

A through-thickness crack was simulated by introducing a gap at the weld bead. In order to consider the crack closure, contact condition was assigned on the crack surfaces. In the crack front, additional refinement was provided. Crack length and load position are shown in **Fig. 4.3**. The crack length was set in the range of 50mm to1000mm in the longitudinal direction. The flanges of the floor beams were fully constrained. Along the two-deck plate boundaries shown in Fig. 4.2, the Y-direction and X-rotation were constrained. Since the crack in this model is located at the center of plate, the boundary condition will not generate significant errors to stresses near crack front.

4.2.2 Load case

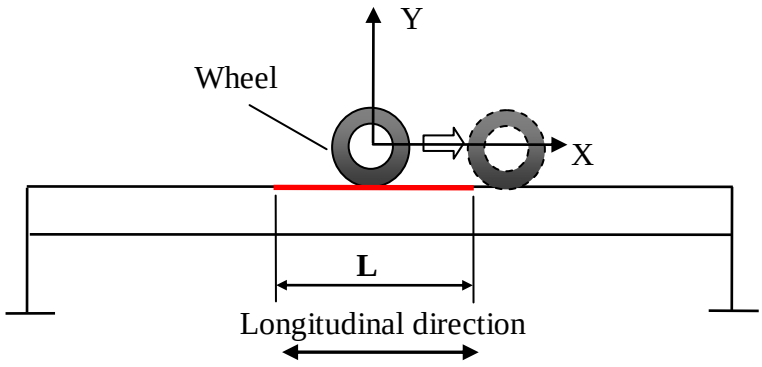

Fig. 4.3 Crack length (L) and load position(X)

In this study, a vertical load of 12kN was applied to an area of 200×200mm as the contact area for a single wheel. In addition, the load distribution due to the pavement was also considered, as shown in **Fig. 4.4** and **Fig. 4.5 (b)**. Assuming solid pavement of 70mm in thickness and a load distribution angle of 45˚, the loading area was set to be 340×340mm for a single wheel, and 340×640mm for double wheels (Xiao et al, 2008). The load is uniformly distributed in the model. Since the contact elements were

provided on the crack surface, the load magnitude can affect the analysis result. However, through a preliminary analysis, it was confirmed that stresses and strains near crack front were almost proportioned to the applied load level.

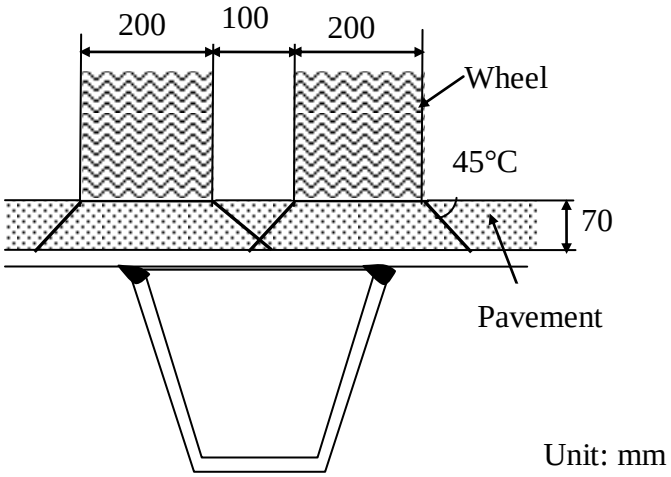

Fig. 4.4 Load distribution due to pavement

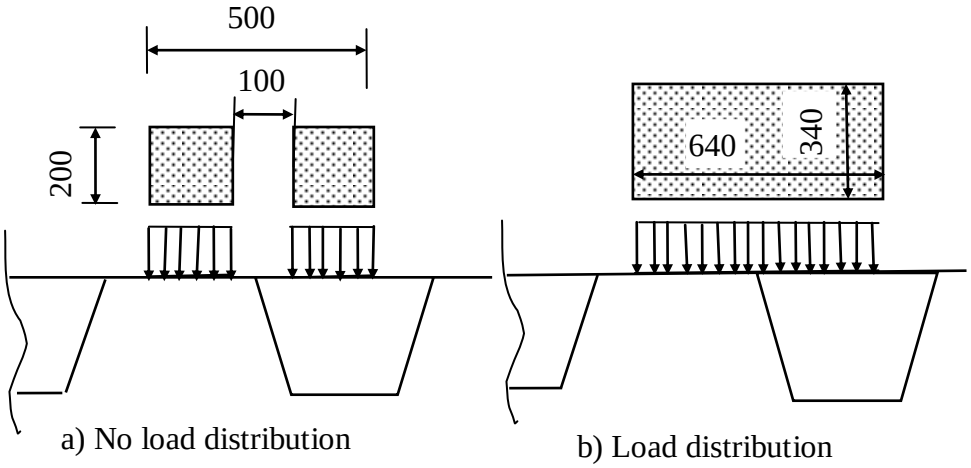

Fig. 4.5 Applied loads Unit: mm

Near the introduced crack, six load cases were applied in the transverse direction (Z-direction in **Fig. 4.1**). For the case without load distribution, three different transverse loading positions (P1, P2 and P3) shown in **Fig. 4.6** were investigated. For the case with load distribution, three positions (P4, P5 and P6) were investigated. In the longitudinal direction (X-direction in **Fig. 4.1**), loading positions listed in **Tabel 4.1** were employed.

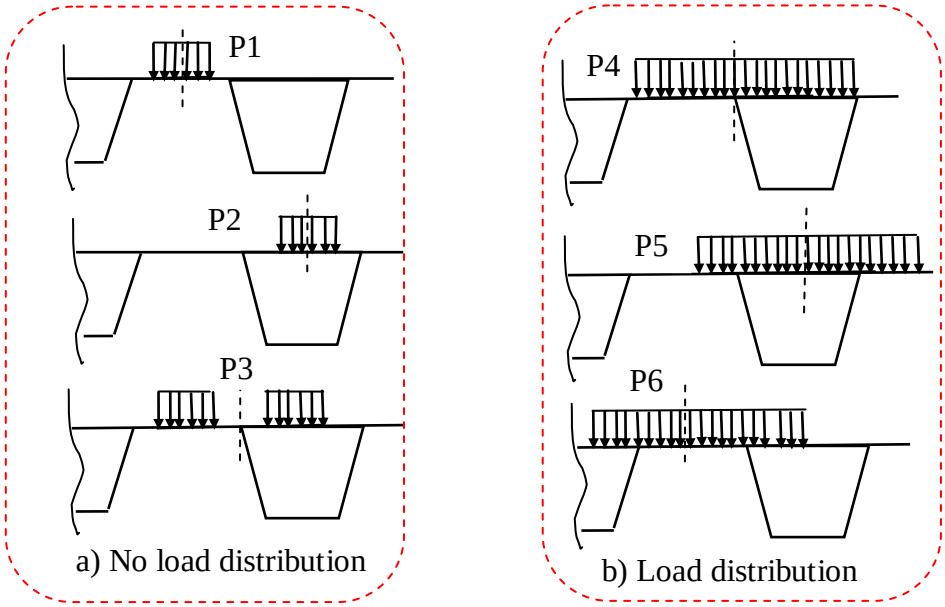

Fig. 4.6 Load case in transverse direction

Table 4.1 Crack lengths and load postions in longidutinal direction

Crack length	50		100		200		300		500		700		1000	
	#	※	#	※	#	※	#	※	#	※	#	※	#	※
Load position in *X*-direction (mm)	0	0	0	0	0	0	0	0	0	0	0	0	0	0
	50	100	50	75	50	75	50	75	75	75	10	10	200	200
	100	150	10	12	10	12	10	17	15	15	20	17	400	325
	125	175	15	17	15	17	15	27	22	22	30	27	500	475
	150	200		22	20	22	20	32	30	32	40	37	600	575
					25	27	25		35	42	45	47	650	675
									40	47	50	52		

Note: *# No load distribution, ※ Load distribution.*

4.2.3 Criterion of crack propagation

The SIF is a parameter that greatly influences the fatigue crack growth. Since the stress field around the crack front has multi-axiality, the mixed deformation mode of Mode I, II and III should be considered. There are several proposals on the crack criteria for crack growth under the mixed-mode condition. Typical crack criteria are the maximum circumferential stress (MCS) criterion (Erdogan and Sih, 1963), the

minimum strain energy density (MSED) criterion (Sih, 1974) and the maximum energy release rate (MERR) criterion (Hussain et al., 1974; Palaniswamy et al., 1978). The MCS criterion can only predict the crack direction for mixed Mode-I and-II. The MSED criterion is also not applicable to three-mode mixed cases, because the Mode-III SIF was considered to have no influece on the crack direction. On the other hand, the MERR criterion has a reasonable basis of energy balance, and is more suitable to apply to three mixed modes. The MERR criterion was proposed by Chang et al. (2006) and validated by comparison with the test results on aluminium alloy specimens under various mixed mode loading conditions. Therefore, the MERR criterion was chosen in this study.

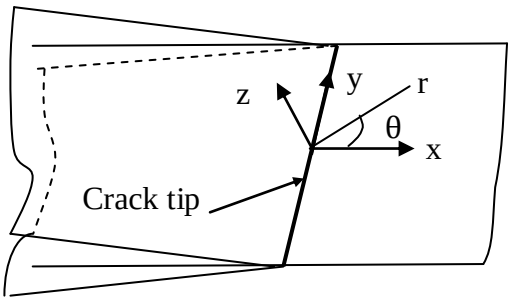

Fig. 4.7 Coordinates near crack front

To establish the fracture criterion based on the MERR concept, the expression of energy release rate must be given. **Fig. 4.7** shows the coordinates near the crack front. The energy release rate in direction θ is given as Equation (4.1)

$$G(\theta) = \frac{1}{2\mu} cos^2 \frac{\theta}{2} \left\{ \frac{\kappa + 1}{8} [K_I^2(1 + cos\,\theta) - 4K_I K_{II}\, sin\,\theta\ + K_{II}^2(5 - 3\,cos\,\theta)] + K_{III}^2 \right\} \quad (4.1)$$

where, G is energy release rate; $\kappa = 3 - 4\nu$ for plane strain, $=(3-\nu)/(1+\nu)$ for plane stress; Ki is SIF of Mode i (i=I,II,III); μ is shear modulus; and ν is Poisson's ratio.

The crack criterion was established as the following equation.

$$\frac{\partial G(\theta)}{\partial \theta}_{\theta=\theta_f} = 0 \left(\frac{\partial^2 G(\theta)}{\partial \theta^2}_{\theta=\theta_f} < 0 \right) \quad (4.2)$$

where, θ_f is the angle corresponding to the maximum of energy release rate.

By substituting Eq. (4.1) into Eq. (4.2), crack criterion was determined as Eq. (4.3).

$$\frac{\kappa+1}{8}\left[K_I^2\left(sin\frac{\theta_f}{2}+sin\frac{3\theta_f}{2}\right)+4K_IK_{II}cos\frac{3\theta_f}{2}-K_{II}^2\left(3sin\frac{3\theta_f}{2}-5sin\frac{\theta_f}{2}\right)\right] + K_{III}^2 sin\frac{\theta_f}{2} = 0 \quad (4.3)$$

In linear elastic fracture mechanics, SIF is most frequenly used to eastimate crack propagation. Therefore, the maximum of the equivalent SIF corresponding to the maximum of energy release rate was expressed as Eq. (4.4):

$$K_{equi} = \left(\frac{4}{\kappa+1}cos^2\frac{\theta_f}{2}\left\{\frac{\kappa+1}{8}\left[K_I^2\left(1+cos\,\theta_f\right) - 4K_IK_{II}\,sin\,\theta_f + K_{II}^2(5-3\,cos\,\theta_f)\right] + K_{III}^2\right\}\right)^{1/2} \quad (4.4)$$

4.3 Estimation of SIF

4.3.1 Extrapolation of SIF

In this study, a displacement extrapolation method (Chan, 1970; Shih, 1976), which is a generally used and relatively accurate method, was employed to calculate the SIFs. The SIF can be estimated by the displacement in the vicinity of the crack. It can be expressed as:

$$\begin{Bmatrix} K_I \\ K_{II} \\ K_{III} \end{Bmatrix} = \lim_{r\to 0}\sqrt{\frac{2\pi}{r}}\begin{Bmatrix} \frac{E\delta_y}{4B} \\ \frac{E\delta_x}{4B} \\ \frac{\mu\delta_z}{2} \end{Bmatrix} \quad (4.5)$$

where, K_I, K_{II}, K_{III} are the SIFs for Mode I, II and III, respectively; $\delta_x, \delta_y, \delta_z$ are relative displacements in *x,y,z* direction; E is elastic modulus; μ is shear modulus; r is distance from the crack tip; and $B = 1 - \nu^2$ for plane strain, =1 for plane stress.

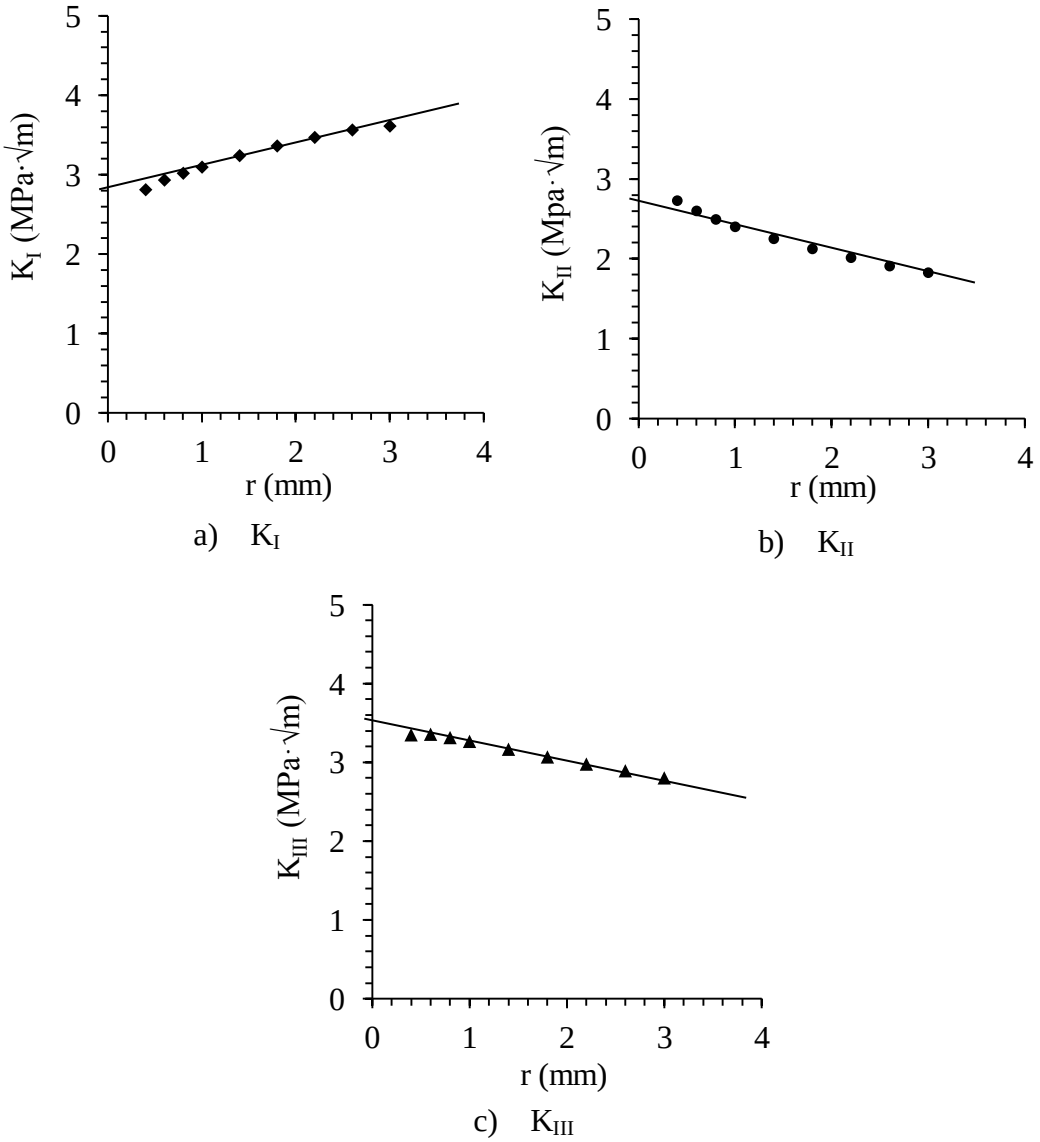

Fig. 4.8 Extrapolation example of the SIF (50mm crack length under P1)

Based on the relative displacements obtained from FEA, the SIF at r=0 can be extrapolated. **Fig. 4.8** shows examples of SIF distribution for Mode-I, II and III. This study estimated the SIF at the crack front based on the SIF distribution across a 3mm range from the crack front, because the FEA results near the crack front are sensitive to element size. For the different crack lengths and load cases, the same method was

employed to calculate SIF. Based on the numerical results of the SIFs of the three modes, the equivalent SIF was evaluated by Eq. (4.4).

4.3.2 Cracking mode

Fig. 4.9 shows an example of K_{equi} along the crack front for the crack length of 700mm when P4 loading is applied at the mid-span ($X=0$ in **Fig. 4.3**). K_{equi} at the weld surface and weld root produce higher values than that at the inner part of the weld bead.

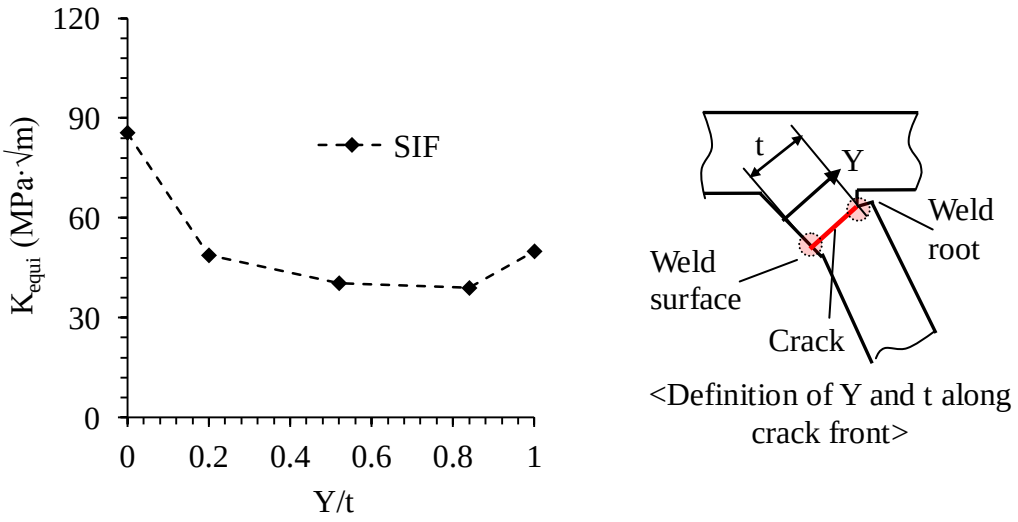

Fig. 4.9 K_{equi} variation along crack front

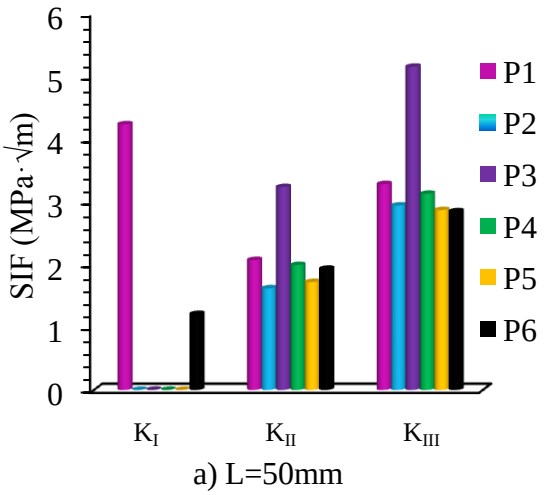

Fig. 4.10 SIFs at the weld root for three crack modes

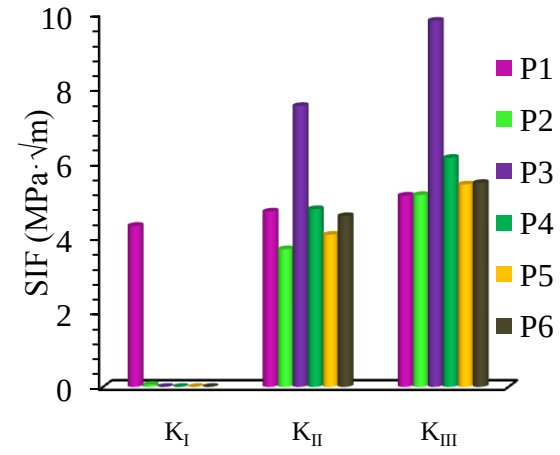

b) L=100mm

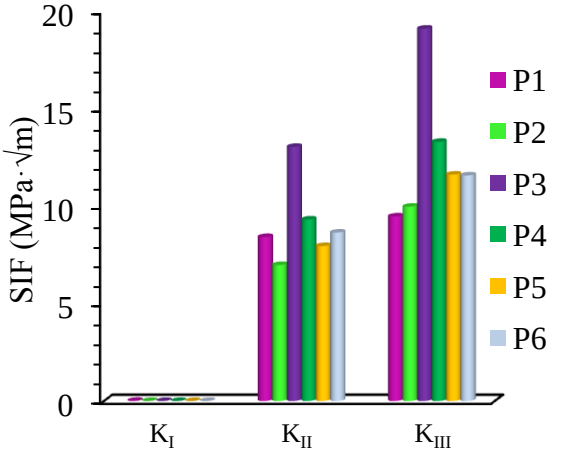

c) L=200mm

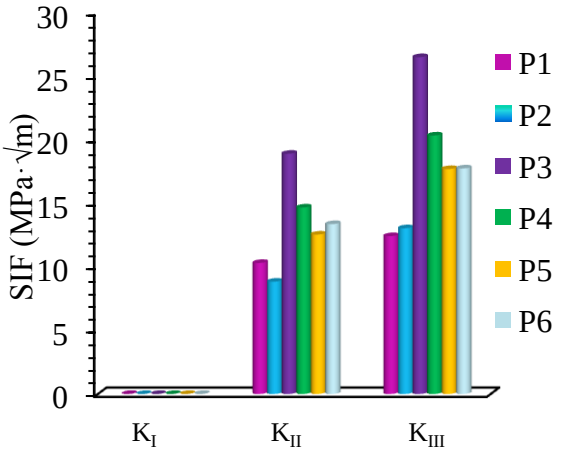

d) L=300mm

Fig. 4.10 SIFs at the weld root for three crack modes(Continued)

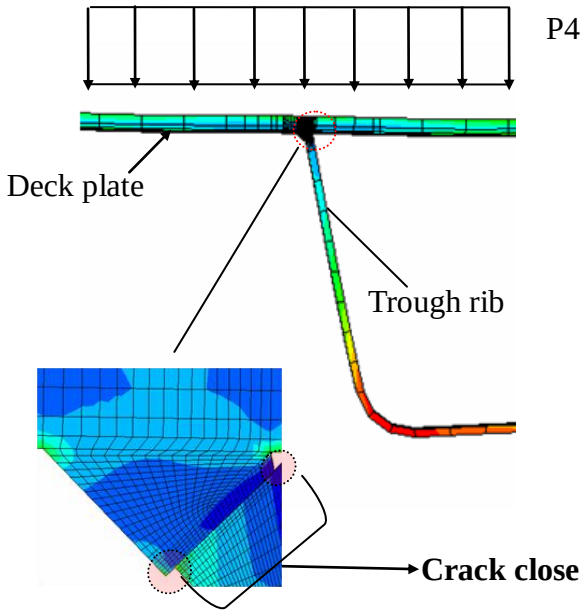

Fig. 4.11 Deformation around crack center under P4

The fatigue crack at the rib-to-deck joint is caused mainly by out-of-plane bending of the deck plate. However, when the crack grows to a certain length, the stress field near the crack front may become complicated due to the complexity of the structure and load condition. **Fig. 4.10** shows the SIFs at the weld root (As shown in **Fig. 4.9**) when the load was applied at the position of X=0mm. When the crack length is 50mm, K_I is relatively large in the load cases of P1 and P6. In the case of P1, K_I is still not zero for the crack length of 100mm. On the other hand, when the crack length is more than 200mm, K_I becomes nearly zero regardless of load cases. Similarly, K_I at the weld surface of the crack front is nearly zero regardless of the load case when the crack reaches to 200mm in length. Deformation near the crack is shown in **Fig. 4.11**. The crack is close because the rib-to-deck weld joint is subjected to compressive load, so that K_I becomes nearly zero when the crack length is over 200mm.

4.4 Equivalent SIF at crack tip

4.4.1 Effect of crack length

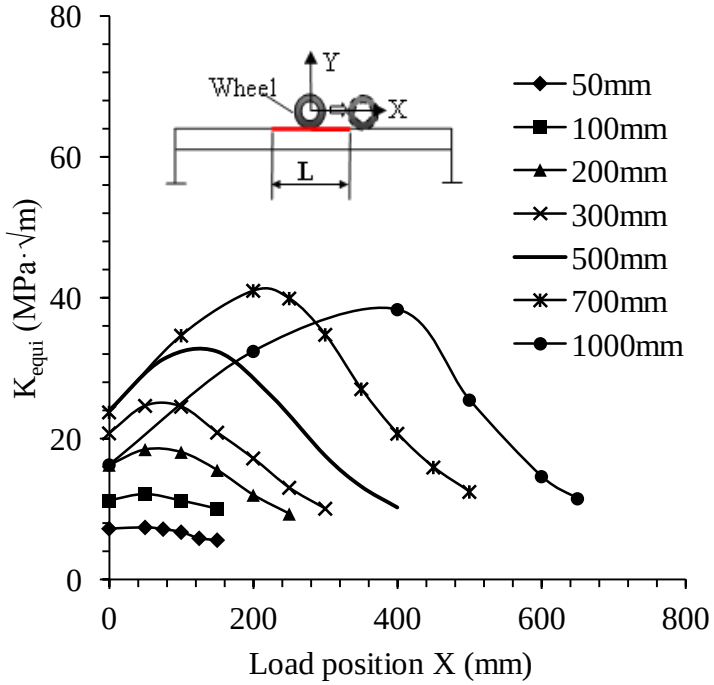

a) At weld root under P1

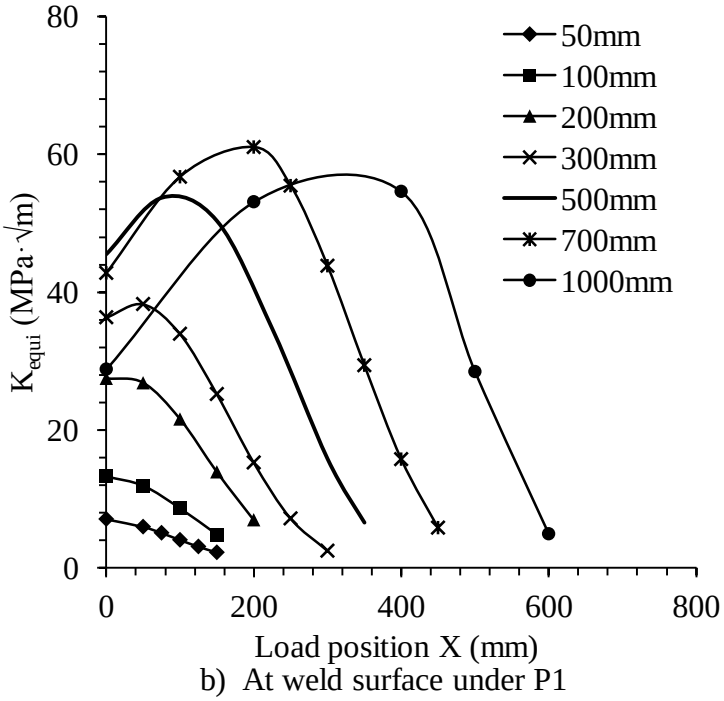

b) At weld surface under P1

Fig. 4.12 Equivalent SIF for P1 and P4 at weld surface and weld root

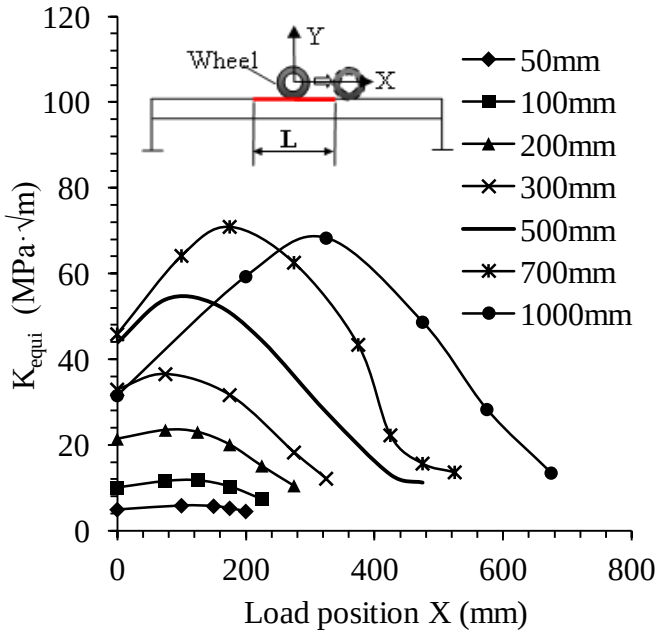

c) At weld root under P4

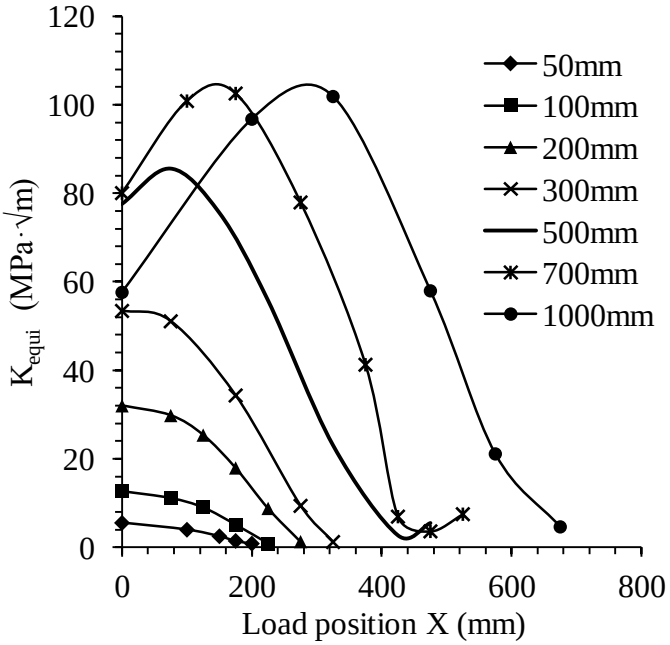

d) At weld surface under P4

Fig. 4.12 Equivalent SIF for P1 and P4 at weld surface and weld root(Continued)

Fig. 4.12 shows examples of the relationships between the equivalent SIF (K_{equi}) and the longitudinal loading position (X). The K_{equi} changes with the longitudinal load positions (X-direction in **Fig. 4.1**). The K_{equi} at the weld surface and the weld root

increases with the increase in crack length until the crack length reaches 700mm, while it becomes smaller with a crack of 1000mm in length. Under the other load cases, the same phenomenon occurs. The maximum K_{equi} at the weld surface appears to be larger than that at the weld root under the same load condition when the crack length is more than 50mm. The same trend also appears for the other load positions.

4.4.2 Effect of load position in transverse direction

Since the double wheels created larger equivalent SIF, only the results for the double wheels load are discussed. In order to investigate the effect of transverse loading position on the SIF, the results for the three load cases (P4, P5 and P6 shown in **Fig. 4.6**) are compared in **Fig. 4.13**. The K_{equi} under P4 is larger than under other loads regardless of the crack length. Therefore, the load location P4 is the most severe load position in the transverse direction. However, the difference of equivalent SIF between P4, P5 and P6 is relatively small. The deformation around the crack center for P4, P5 and P6 (at X=0mm) are shown in **Fig. 4.14**. The similarity of the deformation between them is very high, which results in relatively small differences in equivalent SIF.

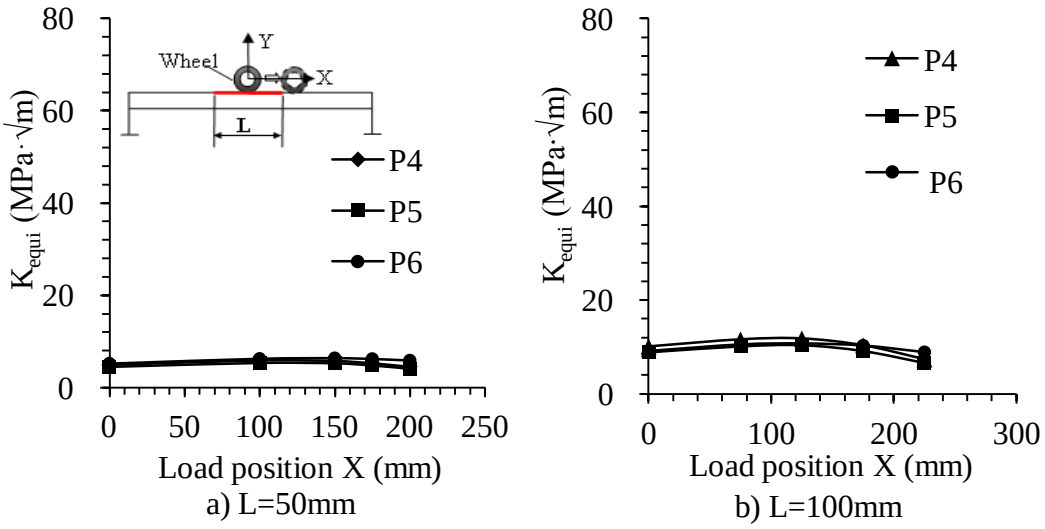

Fig. 4.13 Equivalent SIF for P4, P5 and P6 at weld root

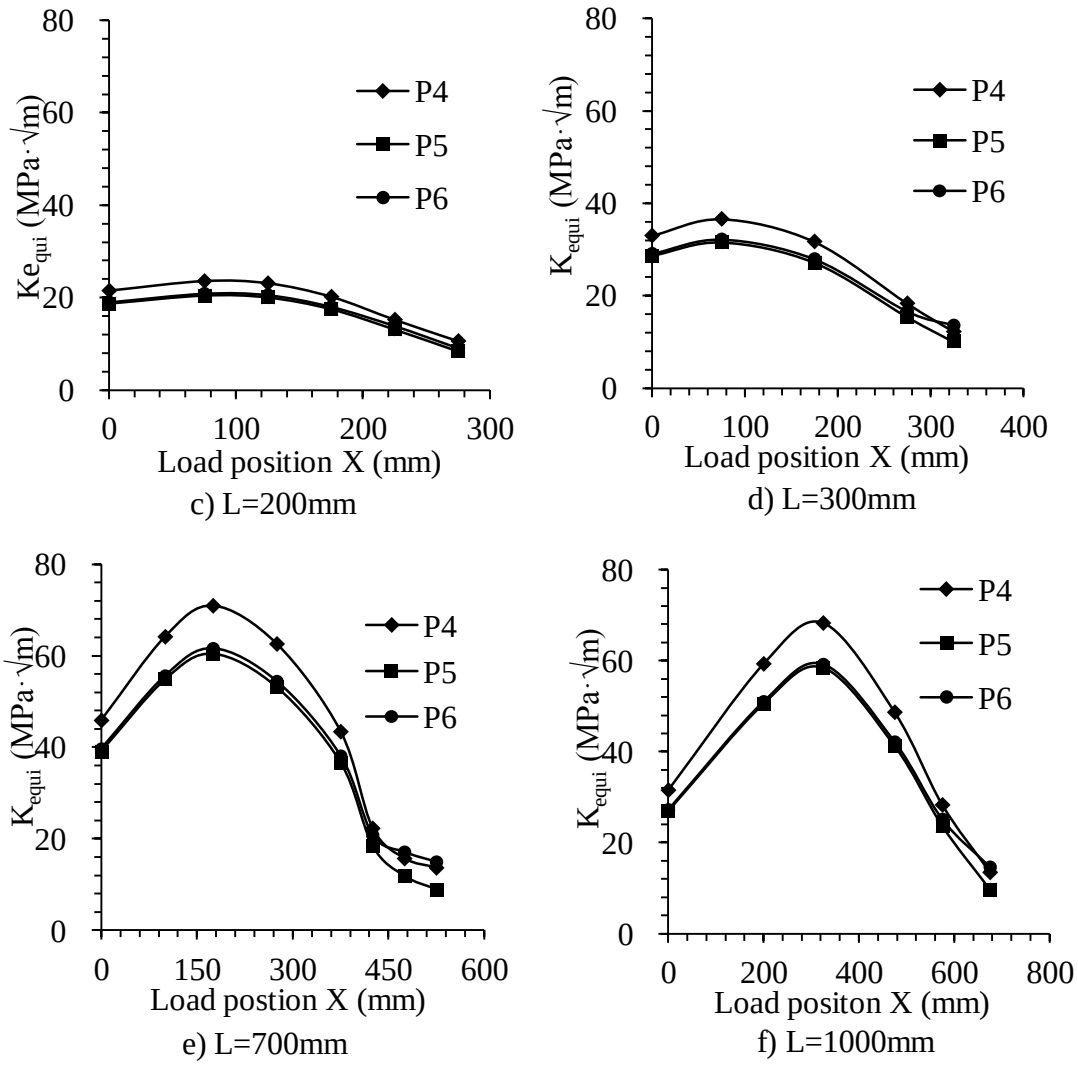

Fig. 4.13 Equivalent SIF for P4, P5 and P6 at weld root (Continued)

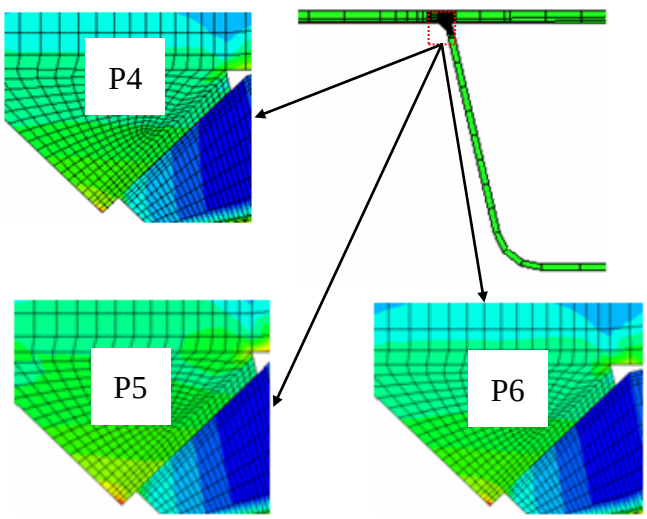

Fig. 4.14 Deformation around crack center for P4, P5 and P6 (stress contour)

4.4.3 Effect of load distribution

In order to investigate the influence of the pavement on the K_{equi}, the results for P3 (no load distribution) and P4 (load distribution) were compared. As examples, the K_{equi} at the weld surface for the cracks of 100, 300 and 500mm are given in **Fig. 4.15**. The maximum K_{equi} under P3 is apparently larger than that for P4. At the weld root, the same K_{equi} pattern was also observed under P3 and P4. Therefore, it can be concluded that load distribution due to pavement can slow down crack propagation.

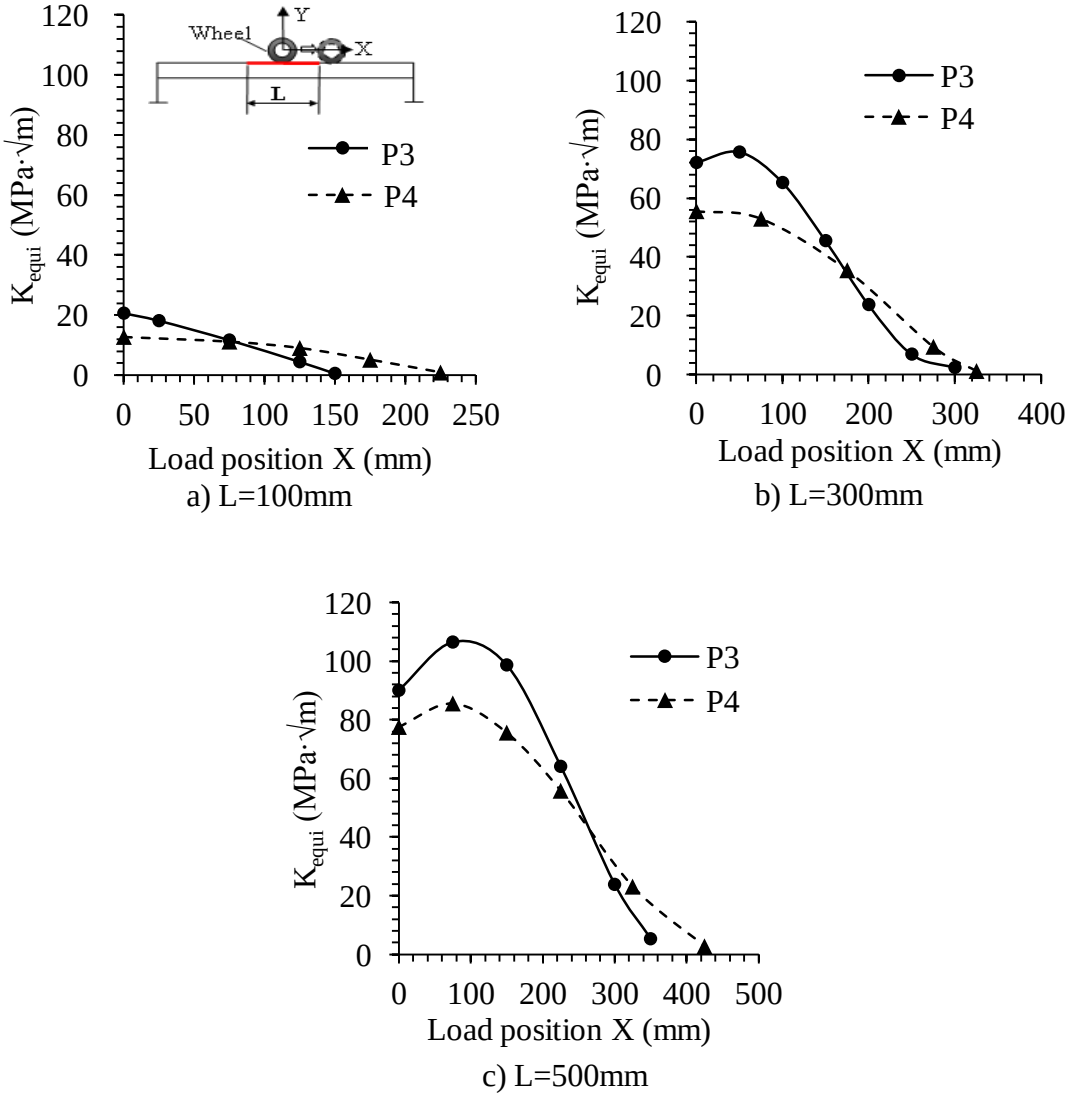

Fig. 4.15 Equivalent SIF for P3 and P4 at weld surface

4.5 Prediction of crack direction

Based on Eq. (4.3), the angle θ_f corresponding to the maximum equivalent stress was calculated. This study assumed took the angle as the direction of crack propagation in the next propagation, called 'crack angle' hereafter. The definition of the crack angle is illustrated in **Fig. 4.16**. The plus crack angle indicates that crack propagates into trough rib, and the minus crack angle indicates that crack propagates into deck plate. Since the K_{equi} for P3 is the maximum result, P3 is the most severe load case in transverse direction. Therefore, the crack direction under P3 is focused on in the discussion.

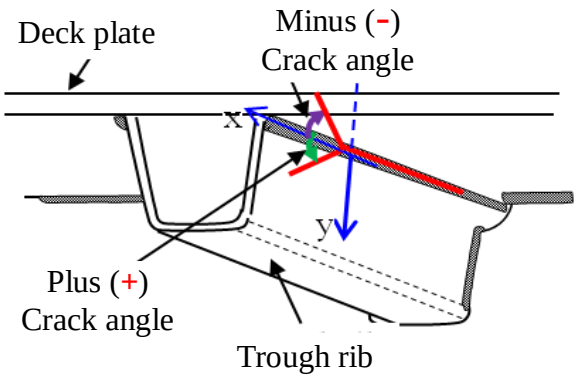

Fig. 4.16 Direction of crack propagation

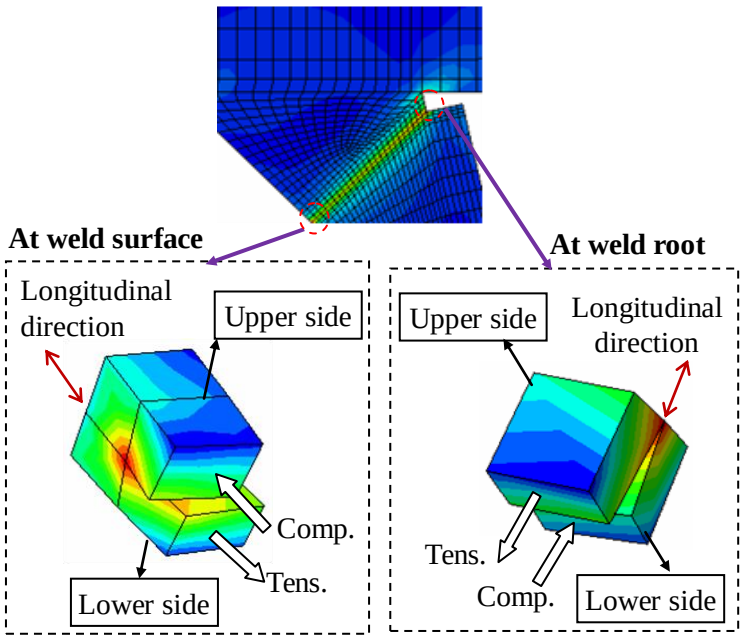

Fig. 4.17 Deformation at two ends of crack tip

The Mode-II deformation has an important effect on the crack angle. **Fig. 4.17** shows the deformation at the weld surface and the weld root. The main deformation modes are Mode-II and-III. The directions of the Mode II deformation at the weld surface and the weld root are reversed. The upper side of the crack is in compression and the lower side is in tension at the weld surface, while at the weld root, the opposite stress pattern can be seen. This is due to the deformation of the rib and the deck plate around the fatigue crack, shown in **Fig. 4.18**. The out-of-plane bending of the rib wall occurring around the cracked area causes the compression on the inner side of the rib wall and the tension on the outer side.

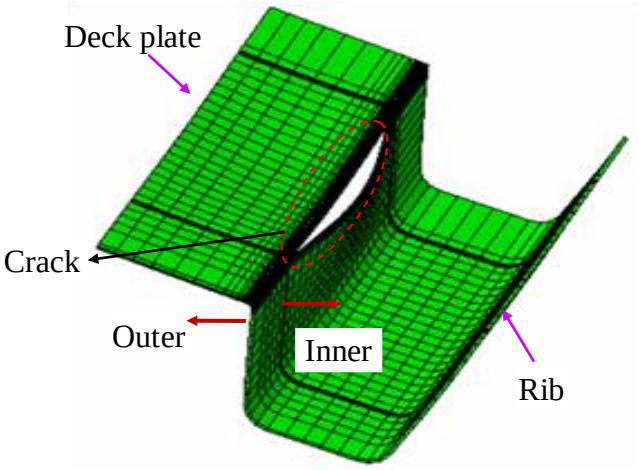

Fig. 4.18 Deformation around fatigue crack

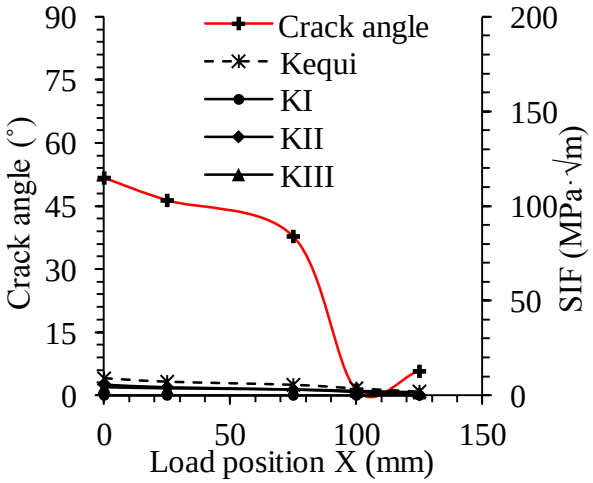

a) L=50mm at weld surface

Fig. 4.19 SIF (K_{equi}, K_I, K_{II}, K_{III}) and crack angle for P3

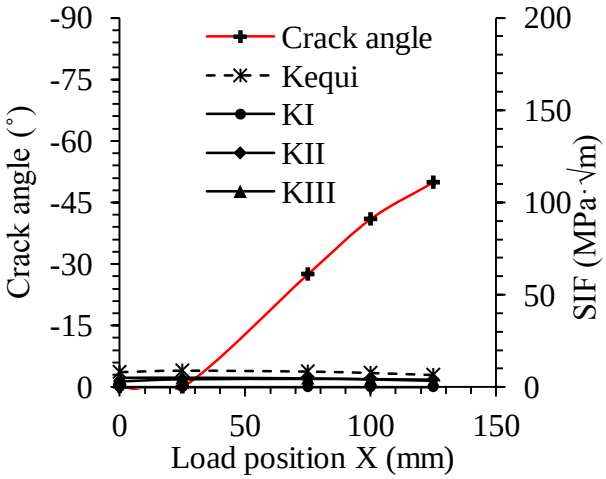

b) L=50mm at weld root

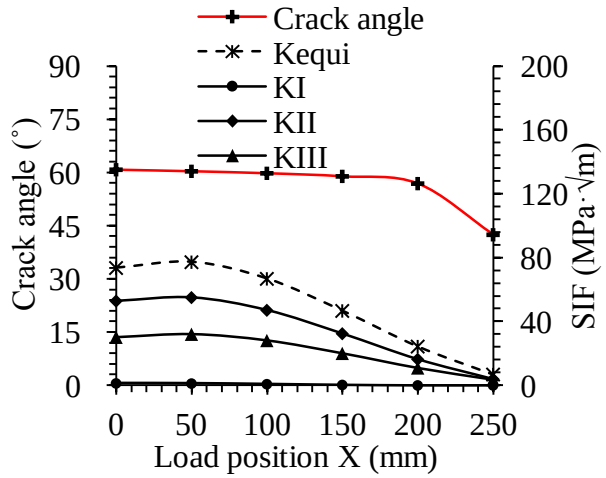

c) L=300mm at weld surface

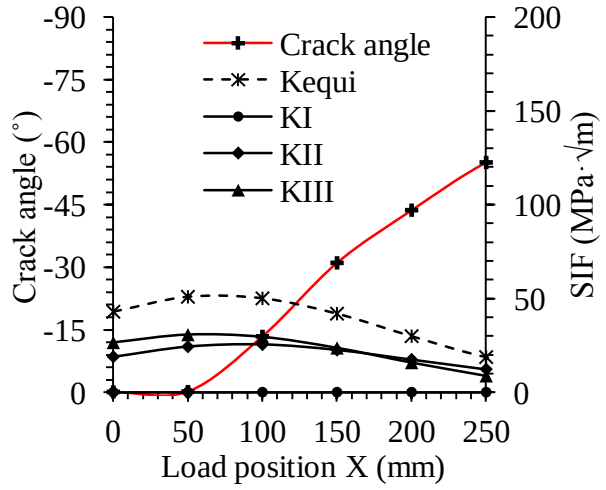

d) L=300mm at weld root

Fig. 4.19 SIF (K_{equi}, K_I, K_{II}, K_{III}) and crack angle for P3 (Continued)

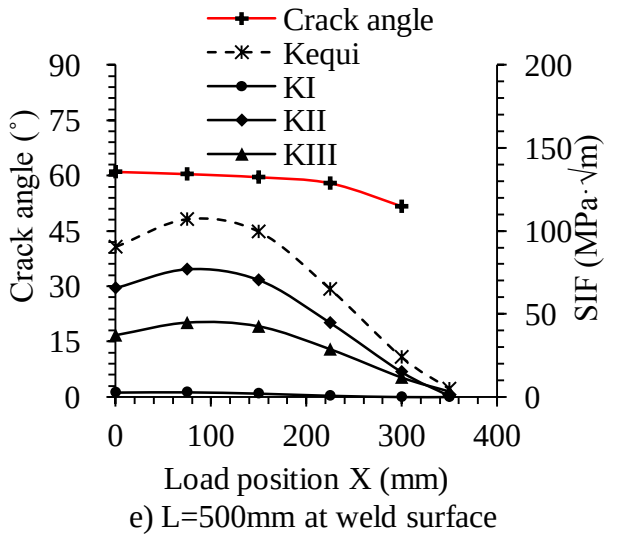

e) L=500mm at weld surface

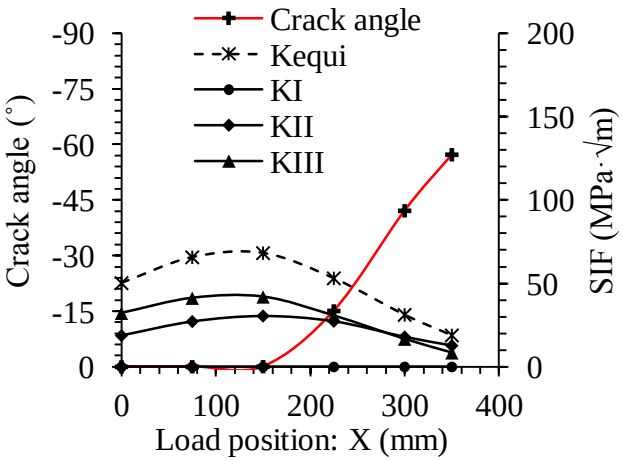

f) L=500mm at weld root

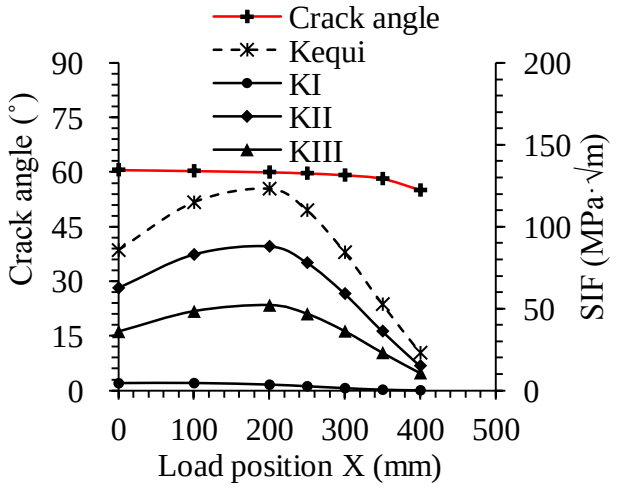

g) L=700mm at weld surface

Fig. 4.19 SIF (K_{equi}, K_I, K_{II}, K_{III}) and crack angle for P3 (Continued)

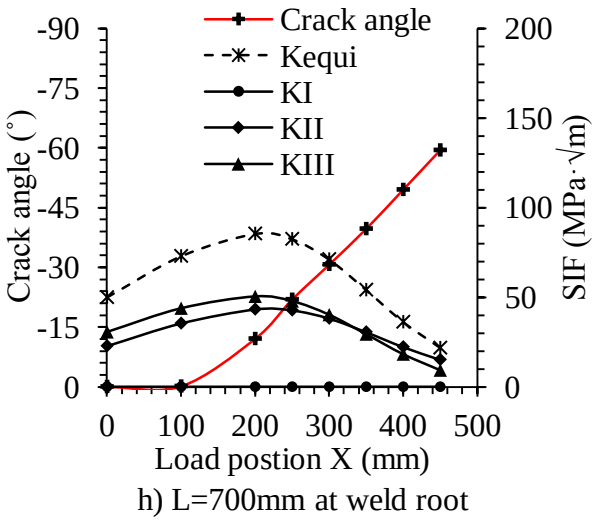

Fig. 4.19 SIF (K_{equi}, K_I, K_{II}, K_{III}) and crack angle for P3 (Continued)

Fig. 4.19 shows the SIFs (K_{equi}, K_I, K_{II}, K_{III}) and the crack angle. As a whole, K_{II} is smaller than K_{III} at the weld root, and K_{II} is larger than K_{III} at the weld surface. It leads to the difference of the crack angle between at the weld surface and at the weld root. Focusing the crack angle, it can be seen that the angles at the weld surface are positive in most cases, which is a possible reason why the crack changes its propagation direction into the rib wall. On the other hand, the angles at the weld root are almost zero or negative. It means that the crack may propagate into the deck plate.

As shown in **Fig. 4.19**, the stress intensity factor and the crack angle are strongly influenced by the longitudinal loading positions. At the weld root, the crack angle corresponding to the maximum K_{equi} is nearly zero when the crack length is less than 700mm, which means that the crack may not change its propagation direction before the crack length reaches 700mm. However when crack length is 700mm, the crack angle corresponding to the maximum K_{equi} is not zero, and the crack could propagate into the deck plate.

At the weld surface, the crack angle is always positive, indicating that the crack is able to change direction at any length. However, crack direction changes just when a crack reaches a considerable length in an actual bridge. Therefore, it does not help to explain actual crack propagation patterns. Further investigation will be needed to reveal

the details of the mechanicsm.

4.6 Conclusion

The reason why a crack at the rib-to-deck welded joint changes its direction into the trough rib was discussed in this chapter. The main conclusions can be drawn as follows:

1) The direction change into the trough rib is related to the Mode-II and Mode-III deformation near the crack tip.

2) In all the load positions investigated in this analysis, the K_{equi} at the weld surface and the weld root do not always increase with the increase in crack length. When the crack length reaches a certain length, the increase in K_{equ} will stop. Additionally, it was also observed that the maximum K_{equi} at the weld surface is larger than that at the weld root under the same load condition when the crack length is very short.

3) The possible patterns of crack propagation direction at the weld surface and the weld root are different. At the weld surface, the crack is able to change its direction into the trough rib wall. At the weld root, the crack is able to change direction into the deck plate. Moreover, at the weld root, until the crack length reaches a considerable length, the crack angle corresponding to the maximum equivalent SIF is still zero, indicating that the crack may not change its direction.

CHAPTER 5

SUMMARIES AND CONCLUSIONS

Some long through-thickness cracks caused by repeated out-of-plane bending stress have been observed in steel bridges. However, it is difficult to apply the concept of fatigue limit state to all fatigue damages in existing steel bridges because they already amount to a huge number. Therefore, to identify how a fatigue crack propagates until the occurrence of brittle fracture, it is necessary to simulate the propagation behavior of relatively long fatigue cracks of at most *X* mm, in some cases more than 1m. This study made efforts to identify the propagation behavior of long through-thickness fatigue cracks under out-of-plane bending. The summary of the research is as follows.

5.1 Conclusion

Chapter 2 examined the SIF distribution along the crack front of a through-thickness crack under out-of-plane bending by using a 3-D finite element analysis. While the SIF distribution along the crack front under tension was nearly uniform across the plate thickness, the SIF under out-of-plane bending was changed across the plate thickness direction due to the effect of the stress gradient and the crack closure on compressive side. This indicates that although the initial crack front is a straight line in the plate thickness direction, the crack-front shape in the next propagation cannot maintain a straight line. In addition, the maximum SIF under pure tension was remarkably larger than that under pure bending.

From the parametric analysis on the cracked plate, it became clear that as the through-thickness crack becomes longer, the influence of the crack closure on the SIF distribution becomes larger. Therefore, to estimate the SIF of through-thickness cracks under out-of-plane bending, the crack closure should be considered in analytical models, especially for long through-thickness cracks. In addition, the plate thickness and the crack length both affect the SIF distribution and the maximum SIF at the tensile plate surface. Although some researchers examined the SIF of through-thickness cracks, the

applied plate thickness was limited to thin plates (less than 5mm), and the crack length was relatively short. Therefore, further studies should be performed for fatigue assessment on long through-thickness cracks observed in steel bridges.

In *Chapter 3*, the propagation behavior of a through-thickness crack under out-of-plane bending was examined by fatigue test. When the stress ratio *R* is zero, the fatigue crack had a quarter-ellipse shape, which is the typical crack shape of a surface crack. Fatigue cracks were observed on both surfaces of the plate except at R=0. In addition, taken as a whole, the crack shapes at R=-0.25, -0.5, and -0.75 were similar to that at R=0. However, in R=-1, the fatigue crack had a symmetrical V shape, which is a unique crack-front shape compared to the other stress ratios. Therefore, FEA was performed on a through-thickness crack with the V-shape crack front. Regardless of the crack length, at R=-1, the SIFs in the tensile region were roughly uniform, declined drastically around the interface of the tensile side and the compressive side, and eventually become zero at the compressive side. Since the SIF range along the crack front was nearly uniform, a correction factor was introduced to express the SIF for a through-thickness crack due to out-of-plane bending. Moreover, through the comparison between the Mode-I SIF and combined Mode-I/III SIF, it was found that the effects from Mode-III loading on crack propagation was negligible in this test.

In *Chapter 4*, a numerical analysis was carried out to investigate why the crack at the rib-to-deck welded joint suddenly changed its propagation direction into the rib wall. By using FEA, the SIF of the through-thickness crack was estimated by the displacement extrapolation method. The propagation direction of the fatigue crack was predicted by the maximum energy release rate criterion. Based on the analysis results, the crack growth mechanism and the reason why the crack changes its direction were discussed. The crack direction change originated from the Mode-II and Mode-III deformation near the crack front. In addition, it was found that the crack propagation direction change can occur at both the weld surface and the weld root. At the weld surface, the crack may change its propagation direction into the trough rib wall. At the weld root, the crack may vary its propagation direction into the deck plate. Moreover, at the weld root, the crack angle corresponding to the maximum equivalent SIF is almost zero until the crack

reaches a considerable length, which indicates that the crack may not change its propagation direction.

5.2 Recommendation for future research

The following recommendations for further study are suggested as follows:

1) In chapter 3, the thickness of the specimen is 15mm, so the proposed correction factor for calculating SIF of through-thickness cracks under out-of-plane bending needs to be verified for different plate thicknesses.

2) In chapter 4, the cause of the crack direction change at the rib-to-deck welded joint in an orthotropic steel bridge deck was investigated by numerical studies. However, it is necessary to verify the analysis results and to identify the mechanicsm in detail through a comparison study with experimentation.

REFERENCES

Alwar, R.S.: Influence of crack closure on the stress intensity factors for plates subjected to bending-a 3-D finite element analysis, *Engineer Fracture Mech.*, Vol.17, pp.323-333, 1983.

Asane, K., Yamaoka. D., and Sakano, A.: Experimental recurrence of the crack through-thickness crack at rib-to-deck weld bead in orthotropic steel bridge deck, *JSCE 66th Annual Conference, pp.162-163,* 2011 (in Japanese).

ABAQUS user manual, version 6.3: Pawtucket, USA: Hibbit, *Karlsson and Sorensen, HKS Inc*; 2002.

Broek D.: Elementary engineering fracture mechanics. AD Dordrecht, The Netherlands: *Kluwer Academic Publishers*; 1986.

Baik, B.: Fatigue behavior of fillet welded joint subjected to bending, *Doctoral Thesis, Nagoya University*, 2008.

Bakker, A.: Three-dimensional constraint effects on stress intensity distributions in plate geometries with through-thickness cracks, *Fatigue Fract. Eng. Mater. Struct.,*Vol.15, No.11, pp.1051–1069, 1992.

Branco, R. and Antunes, F.V.: Finite element modelling and analysis of crack shape evolution in mode-I fatigue Middle Cracked Tension specimens, *Eng. Frac. Mech.*, Vol.75, pp.3020–3037, 2008.

Courtin, S., Gardin, C. and Bezine, G.: Advantages of the J-integral approach for calculating stress intensity factors when using the commercial finite element software ABAQUS. *Engng. Fract. Mech.,* Vol.72, pp.2174–2185, 2005.

Chang, J. and Xu, J.Q.: A general mixed-mode brittle fracture criterion for cracked materials, *Eng. Fract. Mech.,* Vol.73, pp.1249–1263, 2006.

Chan, S.K. and Tuba, I.S.: On the finite element method in linear fracture mechanics. *Eng. Fract. Mech.,* Vol.2, pp.1-17, 1970.

Demepsey, J.P. and Shekhtman, I.I.: Closure of through crack in a plate under bending, *Solids Stru.*, pp. 35, pp.4077-4089, 1998.

Erdogan, F. and Robert, R.: A comparative study of crack propagation in plates under tension and bending, *Proc.1th Int. Conf. Frac.*, Sendai, pp.341-362, 1965.

Erdogan, F. and Sih, G.C.: On the crack extension in plates under plane loading and transverse shear, *J. Basic. Eng.,* Vol.85, pp.519–527, 1963.

Folias, E.S.: On the three-dimensional theory of cracked plates, *J. Appl. Mech.,* Vol.42, pp.663-674, 1975.

Folias, E.S.: Method of solution of a class of three-dimensional elasto-static problems under mode 1 loading, *Int. J. Frac.,* Vol.16, pp.335-348, 1980.

Hwang, C.G., Ingraffea, A.R.: Shape prediction and stability analysis of mode-I planar cracks, *Eng. Fract. Mech.,*Vol.71, pp.1751–1777, 2004.

Hartranft, R.J. and Sih, G.C.: The use of eigenfunction expansion in the general solution of three-dimensional crack problems, *J. Maths. Mech.,* Vol. 19, pp.123-138, 1969.

Hartranft, R.J. and Sih, G.C.: An approximate three-dimensional theory of plates with application to crack problems, *Int. J. Engng. Sci.,* Vol.8, pp.711-729,1970.

Heming, F.S.: Sixth order analysis of crack closure in bending of an elastic plate, *Int. J. Fracture,* Vol,16, pp.289-303,1980.

Izumi, Y.: Detection of through-deck type fatigue cracks in steel deck by self-reference lock-in thermograghy, *The Japan Society of Mechanical Engineering*, Vol.76, pp.723-729, 2010.

Japan Road Association (JRA): *Fatigue design guidelines for steel highway bridges*, Tokyo, 2002 (in Japanese).

Japan Society of Steel Construction (JSSC): Fatigue design recommendations for steel structures and commentary, *JSSC Tech. Rep*. No. 32, Tokyo, 1995 (in Japanese).

Jones, D.P. and Swedlow, I.L.: The influence of crack closure and elasto-plastic flow on the bending of cracked plates, *Int. J. Fracture*, Vol.16, pp.289-303,1975.

Kwon, Y. W.: Finite analysis of crack closure in plate bending, *Compu. Struc.*, Vol.32, pp.1439-1445,1989.

Kwon, S.W., Sun, C.T.: Characteristics of three-dimensional stress fields in plates with a through-the-thickness crack, *Int. J. Fract.*,Vol.104, pp.291–315, 2000.

Kanazawa, T. and Machida, S.: A study of crack propagation and Brittle Fracture in plate with penetrating crack under combined stress, *The Symposium of Japan Society of Naval Architects*, Vol.136, pp.191-205, 1974.

Liu, S.: Tensile-shear transition in mixed mode I/III fracture, *International Journal of Solids and Structures,Vol.4*, pp.6147–6172, 2004.

Miki, C.: Fatigue damage in orthotropic steel bridge deck and retrofit works, *Steel structure*, Vol.6, pp.255-267, 2006.

Miki, C., Suganuma, H., Tomizawa, T., and Machida, F.: Cause study of fatigue damage in orthotropic steel bridge deck, *Journal of Structure mechanics and Earthquake Engineering*, JSCE, No.801/I-73, pp.57–69, 2005.

Mori, T.: Shigihara, S., and Nakamura, H.: Fatigue tests on welded connections between deck plate and trough rib in steel plate deck in consideration of welded penetration, *J. of of Structure Engineering, JSCE*, Vol.62 No.3, pp.570–581, 2006.

Murakami Y, Aoki S, Hasebe N, Itoh Y, Miyata H, Miyazaki N et al.: Stress intensity factors handbook. Berlin: *Pergamon Press*; 1987.

Nagai, A. and Toyosada, M.: A study on the fatigue crack growth in 9% Ni steel plate, *Eng. Frac. Mech.*, Vol.7, pp.481-490, 1975.

Newman, J.C.: A crack opening stress equation for fatigue crack growth, *Int. J. Fract.*, Vol.24, No.3, pp.131–135, 1984.

Nuismer, R. J.: An energy release rate criterion for mixed mode fracture, *Int. J. Fract.*, Vol.11, pp.245–250, 1975.

Owen D.R.J. and Fawkes A.J.: Engineering fracture mechanics: numerical methods and applications. UK: Swansea: *Pineridge press Ltd*; 1983.

Pook, L.P.: The fatigue crack direction and threshold behavior of mild steel under mixed Mode I and III loading, *Int. J. Fatigue,* Vol.7, pp.21-30, 1985.

Shi, G.C. and Macdonald, B.: Fracture mechanics applied to engineering problem-strain energy density fracture criterion, *Eng. Frac. Mech.*, Vol.6, pp.361-386, 1974.

Rice J.R.: A path independent integral and the approximate analysis of strain concentrations by notches and cracks, *J. Appl. Mech.*, Vol.35, No.3, pp.76–86. 1968.

Raju I.S. and Newman J.C.: Stress intensity factors for a wide range of semi-elliptical surface cracks in finite-thickness plates, *Eng. Fract. Mech.*, Vol.11, pp.817–29, 1979.

Rybicki E., Kanninen M.F.: A finite element calculations of stress intensity factors by a modified crack closure integral, *Eng. Fract. Mech.*, Vol. 9, pp.931–938, 1977.

Sih, G.C.: Bending of a cracked plate with an arbitrary stress distribution across the thickness, *J. Engi. Ind. Trans.*, pp.350-356, 1970.

Sih, G.C.: A review of the three-dimensional stress problems for a cracked plate, *Int. J.*

Frac., Vol.7, pp.39-61,1971.

Sih, G.C. and Hartranft, R.J.: Variation of strain energy release rate with plate thickness, *Int..J. Fracture*, Vol. 9, pp.75-82, 1973.

Sih, G.C.: Strain energy density factor applied to mixed mode crack problem, *Int. J. Fract.*,Vol.10, pp.305–321, 1974.

Shih, C.F. and Delorenzi, H.G.: Crack extension modeling with singular quadratic isoparametic elements, *Int. J. Fract.,* Vol.12, pp.647-651, 1976.

Su, X.M. and Sun, C.T.: On singular stress at the crack tip of a thick plate under in-plane loading, *Int. J. Fract.*,Vol.82, pp.237–252, 1996.

Smith, D.G. and Smith, C.W.: A photo-elastic evaluation of the influence of closure and other effects upon the local bending stresses in cracked plates, *Int. J. Frac.,* Vol.6, pp.305-318, 1970.

User manual for Zencrack 7.6: *Zentech International Ltd*. 2005.

Wu, Z.X.: On the through-thickness crack with a curve front in center-cracked tension specimens, *Engineering Fracture Mechanics,* Vol.73, pp. 2600–2613, 2006.

Williams, M.L.: The bending stress distribution at the base of a stationary crack, *J. Appl. Mech.*, Vol. 28, pp.78-82, 1961.

Wu, CH.: Fracture under combined loads by maximum energy release rate criterion, *J. Appl. Mech.*, Vol.45, pp.553–558, 1978.

Xiao, Z., Yamada, K., Ya, S. and Zhao, X.L.: Stress analysis and fatigue evaluation of rib-to-deck joints in steel orthotropic decks, *Int. J. of Fatigue,* Vol.30, pp.1387-1397, 2008.

Ya, S. and Yamada, K.: Fatigue evaluation of rib-to-deck welded joints of orthotropic steel bridge deck, *J. Bridge Eng.*, Vol.16, pp.492-499, 2011.

Ya, S., Yamada, K., Ishikawa, T., and Murai, K.: Fatigue evaluation of trough rib to deck plate joint failed in weld throat, *J. of Constr. Steel of JSSC*, Vol.16 No.64, pp.11–20, 2009.

Yamada, K., and Ya, S.: Plate bending fatigue tests for root crack of trough rib of orthotropic steel deck, *J. of Struct. Eng., JSCE*, Vol.54A, pp.675–684, 2008.

Yuge, T., Machida, F., Morikawa, H., Miki, T., Kamiki, T., and Masui, T.: Analysis of fatigue damage patterns in orthotropic steel deck of Tokyo Metropolitan Expressways, *Proc., Int. Orthotropic Bridge Conf. ASCE*, Reston, VA, pp.531–542, 2004.

Ya, S.: Fatigue durability evaluations of trough to deck plate welded details of orthotropic steel deck, *Doctoral Thesis, Nagoya University*, 2009.

Study on Propagation of Through-thickness Fatigue Crack Subjected to Out-of-plane Bending

A dissertation submitted to the graduate school of engineering of
Nagoya University
in partial fulfillment of the requirements for
the degree of doctor of engineering

By
Xiaochen Ju
July 2012

ACKNOWLEDGEMENTS

Firstly, I would like to express my most sincere and deepest gratitude to my advisor, Professor Kazuo Tateishi, for his constant encouragement and guidance not only in study also in life. Without his patient help and instructive advices, the completion of this thesis would not have been possible. I would like to extend my gratitude to associate professor Takeshi Hanji for giving me many valuable advices in my test and numerical analysis.

I am grateful to the committee members including Prof. Yoshihito Itoh of civil engineering department in Nagoya University and Prof. Masahiro Sakano of Kansai University for providing constructive comments and valuable time for improving the quality of this thesis.

I am grateful to Assistant Prof. Choi. He spent so much time on correcting this thesis. He devoted much energy to my published paper and experiment. Without his support and encouragement, it is difficult for me to finish my doctoral course in time.

Many thanks also go to the former and current members of laboratory including Mr.Tsutiya, Mr.Tsuboi, Mr.Yoshita, Mr.Park. Mr.Ukai, Mr.Nagamatsu, Mr.Sasada, Mr.Kato, Mr.Takase and Mr.Tsuruta and the members of bachelor students for their share of knowledge and their assistance in my fatigue test. I am indebted to many of my friends and all the people who have helped me.

The scholarship provided by Ministry of Education, Culture, Sports, Science and Technology (MEXT) of Japan is gratefully acknowledged.

Last but not least, I must give my special thanks to my parents for their understanding and support.

ABSTRACT

In the high cycle fatigue problem, the fatigue life is generally considered as the numbers until the occurrence of fatigue crack of about dozens of millimeters. It means that small surface crack is considered as the fatigue limit state of steel members. This concept would be appropriate to the fatigue design for newly constructed steel structures. However, it is difficult to apply the concept of fatigue limit state to all of fatigue damages in existing steel brides because the numbers of fatigue damages have already amounted to a huge number, while the budget and the manpower decease gradually. On the other hand, among fatigue cracks, some cracks exist at secondary members, or the crack propagation is under retention state. The risk of fatigue damage is different according to the stress condition of steel member. Therefore, for the reasonable maintenance, it is essential to determine a countermeasure for each fatigue damages based on the understanding of the damage mechanism. Actually, some long through-thickness fatigue cracks have been observed in orthotropic steel decks, which are originated by repeated out-of-plane bending. But, the existing concept of fatigue limit cannot be applied to the fatigue assessment of the long through-thickness fatigue crack. Therefore, this study made efforts to clarify the crack propagation behavior of through-thickness fatigue crack under out-of-plane bending.

Stress intensity factor (SIF) is an essential parameter to identify the crack propagation behavior. The out-of-plane bending condition brings some complexities to estimate the SIF due to gradient stress and crack closure on the compressive side. Although some studies have been performed to estimate the SIF of through-thickness fatigue crack under out-of-plane bending, there are still some important issues to be clarified further. Therefore, this study carried out a 3-D FEA on cracked plate under out-of-plane bending considering the crack closure on compressive side, and the SIF distribution of through-thickness fatigue crack was investigated. As parameters of analysis model, the crack length and the plate thickness were employed in this analysis. The analysis results revealed that the SIF at crack front of through-thickness crack varied in plate thickness

direction under out-of-plane bending, and the SIF distribution along crack front was influenced by the crack length and the crack thickness.

In practical fatigue assessment, it is difficult to perform a numerical analysis corresponding to a steel member. Therefore, some researchers have proposed a simple estimating equation of SIF of through-thickness fatigue crack subjected to out-of-plane bending by assuming the crack front shape as a straight line. However, since the SIF distribution along the crack front varies in plate thickness direction under out-of-plane bending, the crack front may not be a straight line. In this study, as the next step, the crack front shape of through-thickness crack was investigated by fatigue tests on cracked plates. From the fatigue tests, the through-thickness crack had a V-shape crack front under out-of-plane bending, of which the stress ratio was -1. Moreover, based on the experiment result, the SIF along the V-shape crack front was examined in detail by numerical studies.

Finally, because the through-thickness fatigue crack at the welded joint between deck plate and trough rib has been reported, the propagation behavior of through-thickness fatigue crack detected in orthotropic steel deck was investigated by analytical study. The fatigue crack originated by out-of-plane bending sometimes suddenly changes its propagation direction into trough rib. By using FEA, the SIF of the through-thickness crack was estimated by the displacement extrapolation method, and the propagation direction of the fatigue crack was predicted by the maximum energy release rate criterion. Based on the analysis results, the crack growth mechanism and the reason why the crack changes its propagation direction were discussed.

Table of content